

Article

# Analysis of Approaches for Modeling the Low Frequency Emission of LED Lamps

Adam J. Collin <sup>1,\*</sup>, Sasa Z. Djokic <sup>2</sup>, Jiri Drapela <sup>3</sup>, Zekun Guo <sup>2</sup>, Roberto Langella <sup>1</sup> and Alfredo Testa <sup>1</sup> and Neville R. Watson <sup>4</sup>

<sup>1</sup> Department of Engineering, The University of Campania “Luigi Vanvitelli”, 81031 Aversa CE, Italy; roberto.langella@unicampania.it (R.L.); alfredo.testa@unicampania.it (A.T.)

<sup>2</sup> School of Engineering, The University of Edinburgh, Edinburgh EH9 3DW, UK; sasa.djokic@ed.ac.uk (S.Z.D.); Z.Guo-10@sms.ed.ac.uk (Z.G.)

<sup>3</sup> Department of Electrical Power Engineering, Brno University of Technology, 601 90 Brno, Czech Republic; drapela@feec.vutbr.cz

<sup>4</sup> Department of Electrical and Computer Engineering, University of Canterbury, Christchurch 8041, New Zealand; neville.watson@canterbury.ac.nz

\* Correspondence: adam.collin@ieee.org

Received: 31 January 2020; Accepted: 23 March 2020; Published: 31 March 2020



**Abstract:** Light emitting diode (LED) lamps are now an established lighting technology, which is becoming prevalent in all load sectors. However, LED lamps are non-linear electrical loads, and their impact on distribution system voltage quality must be evaluated. This paper provides a detailed analysis of time domain and frequency domain approaches for developing and evaluating models suitable for use in large scale steady-state harmonic power flow analysis of the low frequency (LF) emission of LED lamps. The considered approaches are illustrated using four general categories of LED lamps, which have been shown to cover the vast majority of LED lamps currently available on the market. The aim is an in-depth assessment of the ability of commonly applied models to represent the specific design characteristics of different categories of LED lamps. The accuracy of the models is quantitatively evaluated by means of laboratory tests, numerical simulations, and statistical analyses. This provides an example, for each LED lamp category, of comprehensive information about the overall accuracy that can be achieved in the general framework of large scale LF harmonic penetration studies, particularly in the assessment of voltage quality in low voltage networks and their future evolution.

**Keywords:** component-based model; frequency-domain model; LED lamps; power system harmonics; time-domain analysis

## 1. Introduction

Light emitting diode (LED) lamps are now an established technology and can be utilized in a wide range of applications, from replacing incandescent lamps in residential buildings to the illumination of commercial offices, retail spaces, or industrial premises, as well as street and public area lighting. This wide range of applications, coupled with the well-known advantages in terms of efficiency, regulation of light output, lifetime, and good light quality, have all contributed to the growing market share of LED lamps, which are now prevalent in the residential, commercial, and industrial load sectors. Based on these factors, it is likely that LED lamps will become the ubiquitous lighting technology of the near future. Therefore, it is important to understand the impact of LED lamps on electricity supply networks.

As LED lamps are non-linear electrical loads, their wideband spectrum (i.e., from DC to 150 kHz) current emissions will impact distortion levels in distribution networks. Accordingly, there is

a need to develop accurate models of LED lamps, as an important component of the residential, commercial and industrial load sectors, and power electronic devices in general, as part of ongoing efforts in large scale (e.g., probabilistic) modeling for harmonic penetration studies to assess supply system voltage quality. A vital aspect of ongoing research in this area is the ability to model and simulate the low frequency (LF) current emissions (from DC to 2.5 kHz) of an enormous number of individual devices. Models of LED lamp high frequency (HF) emissions beyond the LF range are not considered in this paper but details of LED lamp HF distortion characteristics are available in [1,2].

Most of the approaches for developing LF harmonic current emission models for large scale steady-state harmonic penetration studies can be divided into two broad categories: time domain and frequency domain. The objective of the time-domain modeling approach is to reproduce the (instantaneous) time domain current waveform of the modeled device, from which further processing is required to extract the LF spectral components. The objective of the frequency-domain modeling approach is to provide the spectral components directly for a given input voltage supply condition.

Time domain models (TDM) are typically based on a representation of the electrical components of the device; when including the control circuits, the modeling approach may be considered as 'white box' modeling, and extensive knowledge of the device is required. Different TDMs for harmonic power flow analyses are available in literature, with a review available in [3] (see References [65–74] of [3]) and other examples in [4–10]. The main advantage of this approach is that the model can be directly applied for the analysis of different supply conditions, i.e., different supply voltage magnitudes and the presence of background voltage distortion, as well as parametric sensitivity analysis. The main disadvantage is that knowledge of the circuit topology is required, while additional knowledge of the control circuits may also be required. With such level of detail it is possible to develop generic models based solely on the required functionality of the power and control circuits, e.g., in [9], or identify specific parameter values to represent a physical device, e.g., [4–8]. However, TDMs usually require a long development time and significant computational resources. Furthermore, specialized software (often not directly compatible with commercial power flow software) is needed, and TDMs are difficult to generalize when modeling a large population of devices, as required for large scale harmonic studies, thus limiting their use. It is possible to overcome some of these disadvantages, e.g., by using an equivalent circuit model to simplify the device representation, e.g., compact fluorescent lamps (CFL) [7] and LED lamps [10], to reduce computation time and the number of model parameters, but limitations still exist.

Conversely, harmonic modeling in the frequency domain can generally be considered either a 'white box' (e.g., Harmonic State Space models [11]) or a 'black box' modeling approach, when knowledge of the circuit topology is not necessary (e.g., Norton-based models). Different frequency-domain models (FDM) for harmonic power flow analyses are available in literature, with a review available in [3] (specifically References [21] and [26–50] of [3]) and, more recently, in [12–15]. Among all of the frequency-domain modeling approaches, Norton-based models are frequently used due to their simplicity and are considered in this paper. Norton-based model can be classified, in order of complexity and accuracy, as: (i) constant harmonic current source models (CCM); (ii) decoupled Norton models (DNM); (iii) coupled Norton models (CNM) [16,17]; and (iv) fully coupled [18,19] or tensor coupled models (T2) [20]. CCMs, which are the most common method used in industry and in commercial software, are not able to reproduce the interactions of the equipment with non-ideal system conditions (i.e., pre-existing background voltage distortion, or common variations in supply voltage magnitude). The last three methods are all based on the use of admittance Frequency Coupling Matrices (FCM) and are suited for linear time invariant systems (DNM) and for linear time variant systems (CNM and T2). Harmonic cross-coupling between voltages and currents of different harmonic orders and the dependency of the harmonic current phasors on the phase angle of the supply harmonic voltage phasors can be modeled by CNM and T2, respectively. Norton-based models have been used to model several power system components and devices [3]. Due to their computational

efficiency, they are preferred for large-scale probabilistic penetration studies [11] and have been used to study the impact of CFLs [21–23] and LED lamps [24] on distortion levels in distribution networks.

From this discussion, it is evident that both model development approaches have certain favorable attributes and have been widely utilized in previous research for modeling the LF current emissions of electrical devices. The development of a TDM can, in theory, start without laboratory measurements, as a generic topology can be readily developed to satisfy a design specification. However, the FDM process must begin from a processed time domain waveform, which can be obtained either from measurement or a TDM. When using measurements as the input, a programmable power source, capable of providing the required voltage supply conditions, is necessary; when using the TDM as the input, its accuracy must be warranted (e.g., experimentally validated).

This paper begins from a thorough critique of the rationale of the development and evaluation process of TDMs and FDMs and considers connections between the two processes. From this critique, the paper then provides a detailed analysis of the time-domain and frequency-domain modeling approaches with the objective of developing and evaluating models of the LF emissions of LED lamps suitable for use in large scale harmonic power flow analysis to assess harmonic distortion in distribution networks. This extends the preliminary research on TDMs [25] and FDMs [26] of LED lamps and fills a gap in existing literature by providing a complete set of models of the four different types of LED lamps suitable for use in harmonic penetration studies. In the analysis, the performance of the models is quantified using experimental data, numerical simulations, and statistical evaluation, providing an in-depth analysis of the ability of commonly applied model approaches to represent the LF emissions of different types of LED lamps. TDMs are utilized to introduce the variation in the circuit topologies present in different types of LED lamps, with different circuit models defined for each type of LED lamp. The TDMs are validated using experimental data from laboratory tests for different supply voltage conditions. In the context of TDMs, a specific contribution of this paper is the proposal of novel models for two of the four types of LEDs, which are presented here for the first time to the best of the authors knowledge. For the purpose of this analysis, the TDMs are used to derive the four Norton-based FDMs, as they allow for rapid development in lieu of extensive laboratory tests. The accuracy of the FDMs is assessed by Monte Carlo (MC) simulation versus TDM results.

Particular attention is given to the FDMs as these are directly applicable for large scale penetration studies, and there is still relatively little information on FDMs of LED lamps. Currently, to the best of the authors knowledge, only two papers consider the widespread impact of CFL or LED lamps in detail [21,24]. The frequency domain analysis demonstrates the impact of the circuit topology on the sensitivity of the device to the background voltage magnitude and phase. The results indicate that, for certain types of LED lamps, the parameter values of the FDM is dependent on the specific background voltage distortion, and the model performance is also influenced by the background voltage distortion present in the supply voltage. This novel contribution to the FDM area provides comprehensive information about the overall accuracy of the FDM when representing different LED lamps, serving as a guide on the impact of model selection on the assessment of voltage distortion in low voltage (LV) networks. All TDM parameter values are included in Appendix A for use by the community; from these models, all FDM parameters, which are difficult to communicate in compact form, can be derived. However, FDM models are available from the authors upon request.

The rest of the paper is structured as follows: a rationale of the development and evaluation of TDMs and FDMs is discussed in Section 2; the TDM approach is analyzed in Section 3, the FDM approach is analyzed in Section 4; conclusions are provided in Section 5.

## 2. Rationale of the Development and Evaluation of Time and Frequency Domain Models

TDMs and FDMs can be developed, and their performance assessed, following different processes. Figure 1 highlights the general processes and input data requirements of the time-domain and frequency-domain modeling methodologies. The time-domain modeling methodology implemented in this paper is denoted by the blue path, with the frequency-domain modeling

methodology shown by the orange path. Use of the physical device, i.e., the LED lamp to be modeled, is marked by the black path. In the approach implemented in this paper, the lamp under test serves as the starting point for the TDM, which in turn serves as the input for the subsequent development of the FDM. The alternative path for FDM development, marked in grey, indicates that modeling in the frequency domain can also start directly from the physical device. This path has the inherent advantage that any inaccuracies present in the TDM do not propagate to the FDM, but it requires a fully controllable power source for laboratory testing and a huge number of test points.

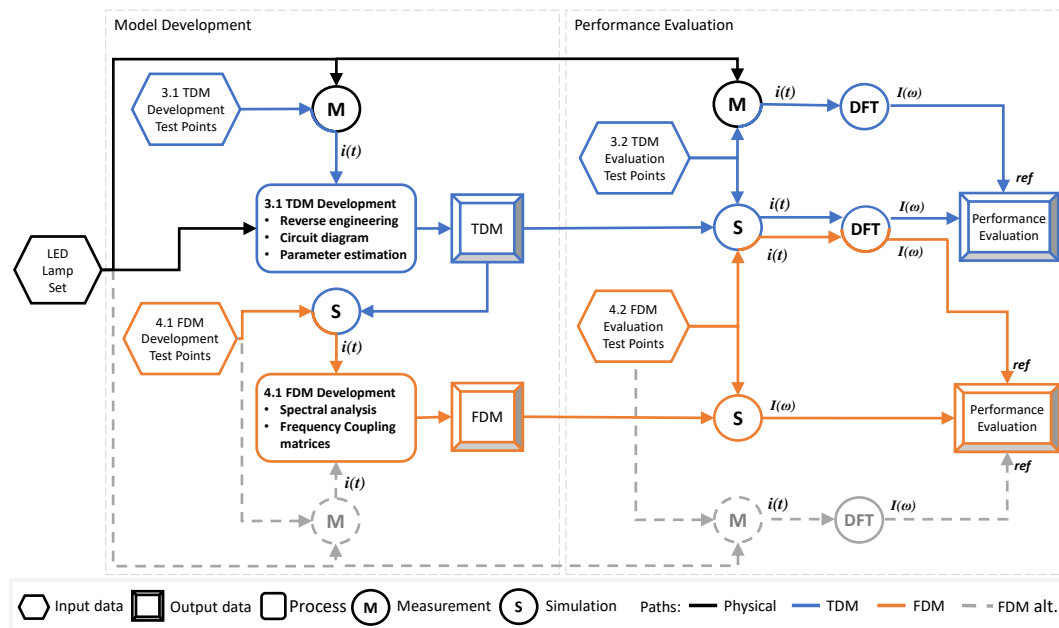


**Figure 1.** Rationale of the development and performance evaluation of time-domain models (TDMs) and frequency-domain models (FDMs). LED = light emitting diode.

The whole process can be divided into two main stages: model development and model performance evaluation. The model development process involves defining a model structure and obtaining the parameters of the lamp under test. It should be noted that, although presented for LED lamps, the comprehensive analysis of modeling processes in Figure 1 is generally applicable for modeling the LF emissions of any electrical device. Clearly, the required steps are significantly different for the development of TDMs and of FDMs. However, the model development process is specific to the properties to be emulated correctly and the specified range of operating conditions. In this paper, attention is devoted to the LF harmonic content of line current waveforms of common LED lamps, subjected to supply voltage deviations from rated sinusoidal conditions.

For performance evaluation, the specification of the test points is given in terms of the supply voltage distortion and requires a formal definition of the magnitude and phase of the frequency components of the voltage waveforms used in the evaluation process. These are marked as separate processes in Figure 1, as different evaluation test points are implemented in this paper for TDMs and FDMs to illustrate different possible approaches for model performance evaluation. However, the same test points could be used for TDM and FDM cases to directly compare the accuracy of the different modeling approaches.

In the remainder of this section, the parts common to both time domain and frequency modeling methodologies are introduced. These are: the LED lamp set, which serves as an input to the whole process; the characteristic voltage waveforms for test point definitions, which are an input to the model evaluation process; and the model evaluation metrics. Specific details of the development and the evaluation stages utilized for the time-domain and frequency-domain modeling methodologies are found in the subsequent sections, with relevant subsection numbers marked in Figure 1.

## 2.1. LED Lamp Set

Recent work on power quality issues caused by LED lamps, e.g., [1,27], has revealed the diversity in the LF current emissions of LED lamps. These variations are a consequence of the utilization of different LED driver circuits, and previous research has shown that, for the purpose of classification of the LF emissions of the line current waveform, LED lamps can be divided into four main categories [28]. The categories are based on the circuitry utilized to convert the AC supply voltage to the DC current required by the LED chain and are defined as follows:

- Type A: consists of a full-wave rectifier with bulk smoothing capacitor and DC-DC switch-mode converter;
- Type B: consists of a simple capacitor divider formed across a full-wave rectifier circuit;
- Type C: consists of a full-wave rectifier loaded by a constant current regulator (CCR);
- Type D: includes a switch-mode driver circuit with active power factor correction (aPFC), which can be either a single-stage or a double-stage converter.

One LED lamp from each type was selected for the model development process. The line current waveforms of the four LED lamps considered in this research, which are typical for each category, are shown in Figure 2. Table 1 provides the main electrical data obtained from measurements of the lamps considered with rated sinusoidal AC voltage waveform. A comprehensive description and classification of the LED lamp driver circuits is available in [29,30].

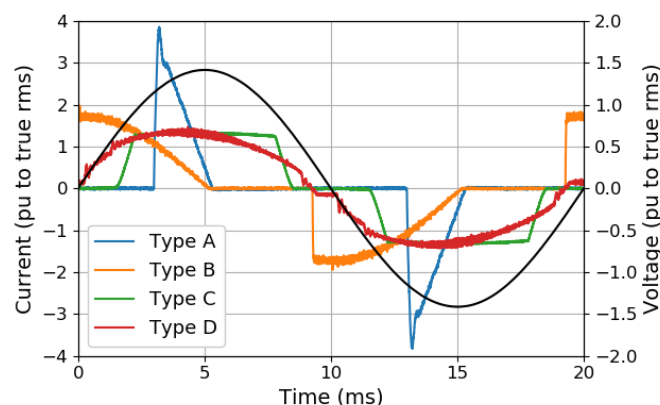


**Figure 2.** Line current waveforms of the LED lamps at rated sinusoidal voltage, where each lamp is normalized with respect to its true rms value.

**Table 1.** Main electrical data of the considered LED lamps at rated sinusoidal voltage.  $PF_1$  = fundamental power factor; THD = total harmonic distortion; THC = total harmonic current.

Type (-)	Power (W)	$PF_1$ (-)	THD (%)	THC (mA)
A	5	0.93	139	32.3
B	4.5	0.44	49	21.6
C	13.6	1.00	28	16.4
D	40	0.98	8	14.4

## 2.2. Characteristic Voltage Waveforms for Test Points Definition

The definition of test points for the development and performance evaluation of both modeling approaches is based on three characteristic voltage waveforms, selected as representative base case conditions of typical voltage distortion in Low Voltage (LV) networks [31]. The three different voltage waveforms considered are shown in Figure 3. The sinusoidal voltage waveform is considered as an ideal supply, which is particularly important for the development of TDMs. The flat top (FT) and peak top (PT) voltage waveforms are selected as representative of the typical voltages present in low-voltage networks, the total harmonic distortion (THD) values are 3.0% and 3.6%, respectively.

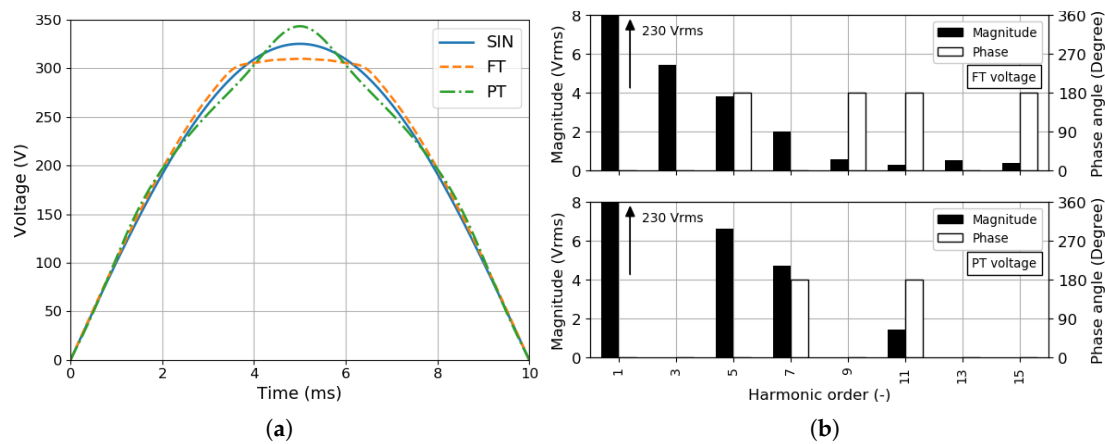


**Figure 3.** Characteristic voltage waveforms (sinusoidal (SIN), flat-top (FT), and peak-top (PT)) at rated voltage magnitude: (a) Time domain (SIN, FT, and PT). (b) Frequency domain (FT and PT).

### 2.3. Model Performance Evaluation

Different performance evaluation procedures are implemented for time-domain and frequency-domain modeling approaches, with full descriptions included in Sections 3.2 and 4.2, respectively. However, the performance evaluation metrics are identical for both modeling approaches and focus on the deviations of the LF current components from the reference values.

The magnitude errors are quantified using the relative percentage error:

$$\epsilon_{mag,h} = \frac{\left| |I_{h,est}| - |I_{h,ref}| \right|}{|I_{h,ref}|} \times 100, \quad (1)$$

and the phase errors are quantified using the absolute error:

$$\epsilon_{phase,h} = \left| \angle I_{h,est} - \angle I_{h,ref} \right| \quad (2)$$

for  $h = 1, 3, \dots, H$ , where  $I_{h,est}$  is the estimated current value of order  $h$ , and  $I_{h,ref}$  is the reference current value of order  $h$ . As indicated in Figure 1, the measurement data is used as  $I_{h,ref}$  in the TDM process, while the TDM serves as  $I_{h,ref}$  during the FDM analysis. In this paper, odd harmonics up to and including the 15th order are considered, i.e.,  $H = 15$ .

In addition to the assessment of individual harmonic components, THD and total harmonic current (THC) indicators are also evaluated:

$$THD = \frac{\sqrt{\sum_{h=3}^H |I_h|^2}}{|I_1|} \times 100, \quad (3)$$

$$THC = \sqrt{\sum_{h=3}^H |I_h|^2}. \quad (4)$$

The THD and THC provide aggregate information about the overall harmonic content in the line current drawn by the LED lamp and are especially valuable when evaluating the model performance across different LED lamps and categories. For TDMs, the THD and THC error are calculated in absolute terms; for FDMs, the THD and THC errors are calculated in relative terms for quicker comparison between the multiple model forms.

All evaluation metrics are presented using boxplots, in order to summarize the significant statistical indices from numerical values obtained using the evaluation test points (described in Sections 3.2 and 4.2, respectively) in a concise manner. For each box, the central mark is the median,

the edges of the box are the 25th and 75th percentiles, and the whiskers extend to the most extreme data points ( $\pm 2.7\sigma$  and 99.3% coverage if the data are normally distributed), not considering outliers.

### 3. Time Domain Models

#### 3.1. Time Domain Model Development

When developing a model to emulate a real world process, e.g., start-up, steady state, regulation, failure, etc., there are a wide range of influencing parameters, e.g., various supply conditions, and a very detailed model may be required. Therefore, it is important to clearly define the specific response to be emulated, and the particular conditions for which the model is valid, in order to simplify the model development process. Typical techniques employed to simplify the model are idealization, linearization, and averaging, and simplified models should include the key components, either directly or as equivalents, which allow for the desired response to be obtained.

The general procedure for developing a TDM consists of two main stages:

1. In the first stage, the key components of the topology and functionality of the circuit should be identified. This can be achieved by reverse engineering of the lamp or using a priori knowledge of the relationship between current waveform shape and specific circuitry;
2. In the second stage, values for the key components should be obtained. This can be performed either by reverse engineering of the lamp or by a parameter estimation technique.

The Type A LED model is developed using a priori knowledge of the relationship between the measured line current waveform shape and commonly utilized driver topologies. The component values of the circuit are obtained by a parameter estimation technique, with further details in [32,33]. As the circuits employed in Type B and Type C LED lamps consist of only a few components, the circuit structure was identified by reverse engineering. For the Type B LED lamp, Step 2 was performed directly using the physical components, while the parameters were estimated for the Type C LED lamp. Reverse engineering was also applied to develop the Type D LED lamp model in Step 1, followed by tuning the control circuit parameters to match the simulated input line current with the available measurements. Unlike the Type A LED lamp, simplification of the control algorithms of Type D LED lamp is difficult to achieve and a generic equivalent circuit model does not exist.

The TDMs were implemented in MATLAB/SIMULINK, with the exception of the Type D LED lamp model, which was developed in PLECS. The circuit schematics and component values used in this paper are available in Appendix A. All experimental data from laboratory tests were obtained with negligible source impedance; further details of the measurement chain are available in [28]. In consonance with this, the voltage source equivalent internal impedance was neglected during the simulation of the TDMs.

#### 3.2. Time Domain Model Evaluation

The TDMs were evaluated at a number of test points by comparing the magnitude and phase angle of the current harmonics obtained using the TDM against the values extracted from measurement data under the same supply conditions. The measurement data is taken as  $I_{h,ref}$  in Equation (1) and (2), with the TDM output taken as  $I_{h,est}$ . To obtain the harmonic components from the time domain line current waveforms, the waveforms are processed by Discrete Fourier Transform (DFT) using a 200 ms rectangular window, in accordance with [34].

In this paper, the TDM test design considers a set of five magnitudes of the voltage fundamental  $V_{1,pu} = \{0.90, 0.95, 1.00, 1.05, 1.10\}$  for each of the voltage waveforms in Section 2.2. For each magnitude of the voltage fundamental, the harmonics shown in Figure 3 are scaled proportionally, thus maintaining a fixed THD level. These 15 test points are considered sufficient for evaluating the steady-state performance of the TDM developed for each type of LED lamp defined in Section 2.1. Additional test points could be included depending on the level of certainty required.

For the presentation of the results, there is no discrimination by voltage magnitude nor waveform shape. This is possible as there is little correlation between the supply condition and the model performance. However, this does have an effect on the FDMs, which is discussed further in Section 4.

### 3.3. Results

#### 3.3.1. Type A

The assumed circuit model structure and the values obtained from the parameter estimation technique are included in Appendix A.1. Appendix A.1 also includes the model validation at the development test point, i.e., at rated ideal sinusoidal voltage.

A comparison of the range of harmonic current magnitude and phase angles obtained from the developed model and the measured data across all considered test points is shown in Figure 4, where the excellent performance of the model is observed. This is expected as the assumed equivalent circuit model is an established approach to modeling such electronic loads. Generally, the magnitude and phase angle errors increase with harmonic order, i.e., in inverse proportion to the magnitude of the current harmonic. Phase angle dispersion, which also increases with harmonic order, is caused by the sensitivity of the load to changes in the supply voltage waveform. However, as demonstrated by the low value of the phase errors, the TDM is able to accurately reproduce this behavior.

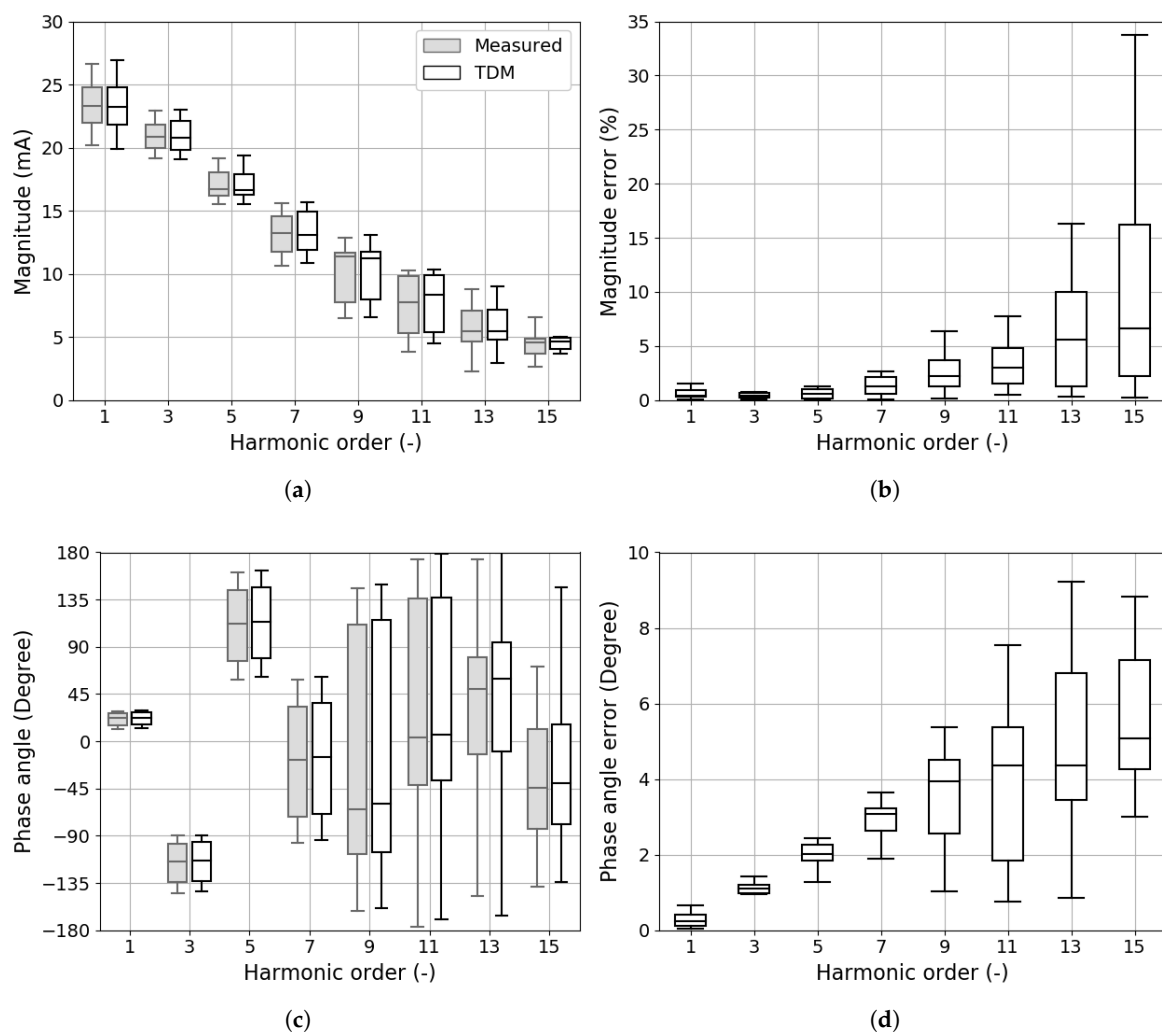


**Figure 4.** LED Type A: Comparison of the time-domain model (TDM) and the measured data for all test points: (a) Magnitude; (b) Magnitude error; (c) Phase angle; and (d) Phase angle error.

### 3.3.2. Type B

The assumed circuit model and its parameterization are included in Appendix A.2. Due to the simple nature of the circuit topology, all components are explicitly represented in the model. Appendix A.2 also includes the model validation at the development test point, i.e., at rated ideal sinusoidal voltage.

A comparison of the range of harmonic current magnitude and phase angles obtained from the developed model and the measured data across all considered test points is shown in Figure 5. Again, the accuracy of the developed TDM is very high, with magnitude errors comparable to those observed for the Type A LED lamp (c.f. Figure 4). However, unlike the Type A LED lamp, the value of the magnitude error is not simply correlated to the harmonic order. Although larger phase angle errors are observed than in the case of the Type A LED lamp, the median values are all below  $20^\circ$ , with lower values reported for the prominent harmonic tones.

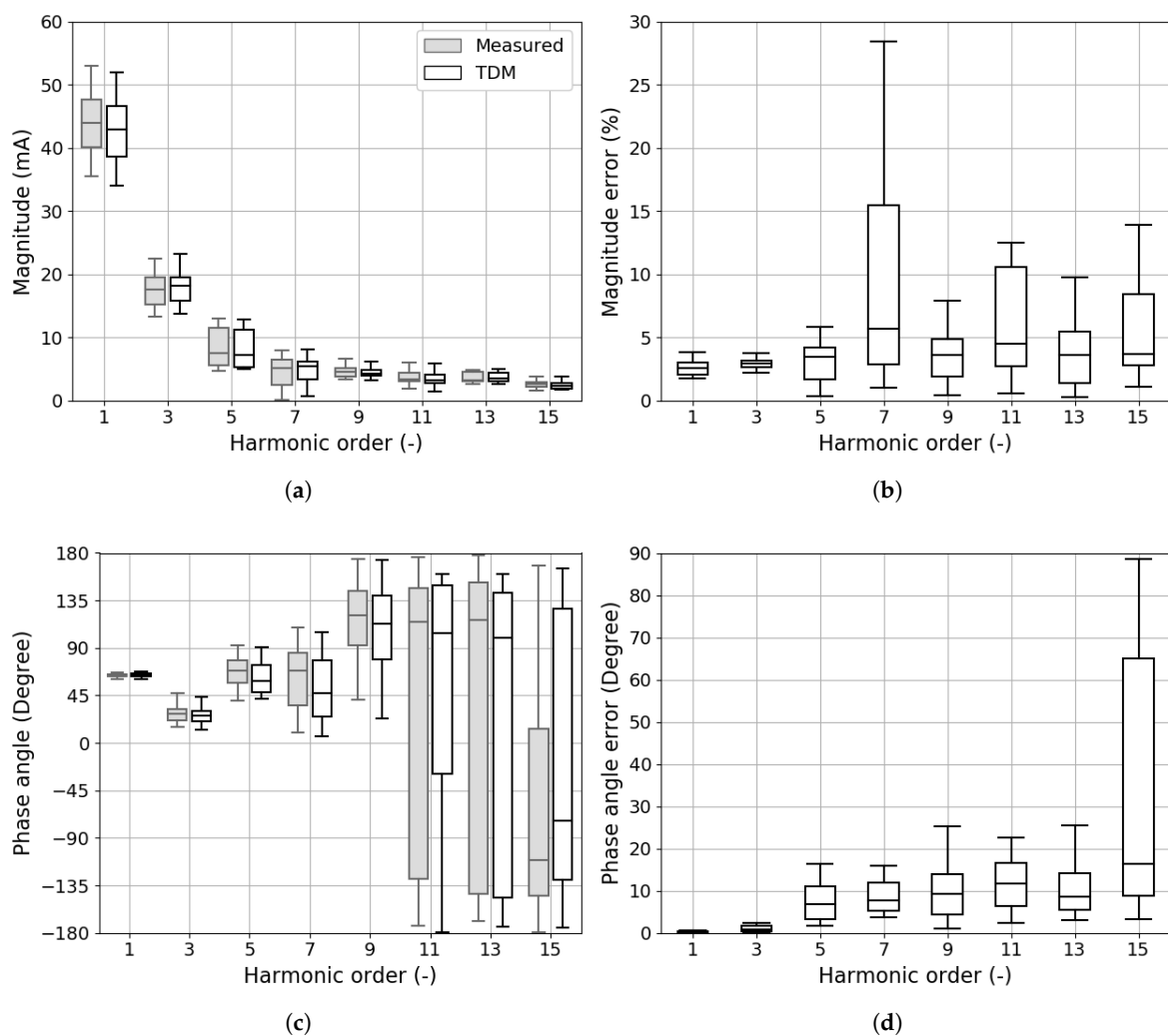


**Figure 5.** LED Type B: Comparison of the time-domain model (TDM) and the measured data for all test points: (a) Magnitude; (b) Magnitude error; (c) Phase angle; (d) Phase angle error.

### 3.3.3. Type C

The assumed circuit model and parameter values are included in Appendix A.3 and is presented for the first time in this paper. Appendix A.3 also includes the model validation at the development test point, i.e., at rated ideal sinusoidal voltage. The comparison of the range of harmonic current magnitude and phase angles obtained from the developed model and the measured data across all considered test points is shown in Figure 6.

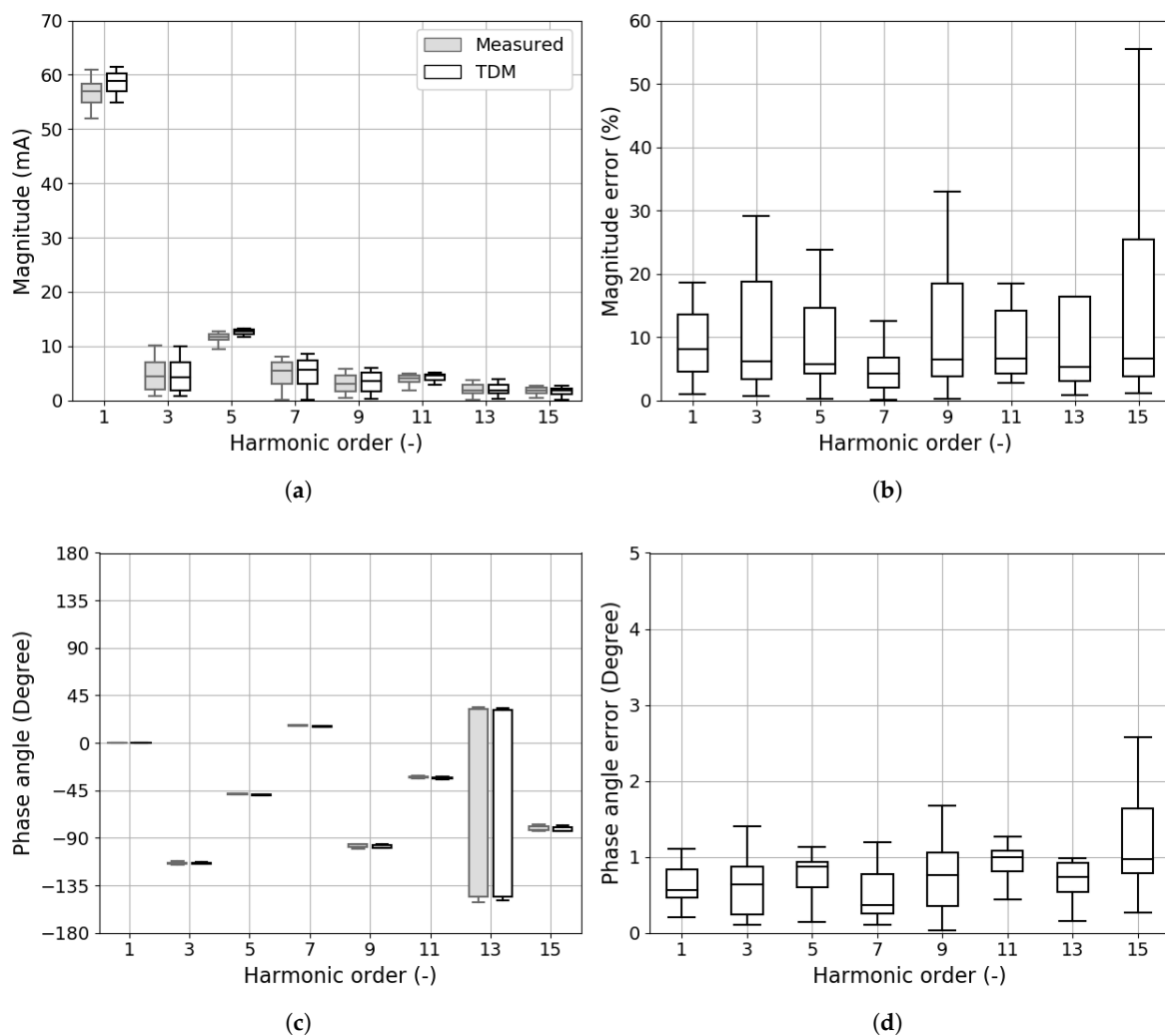


**Figure 6.** LED Type C: Comparison of the time-domain model (TDM) and the measured data for all test points: (a) Magnitude; (b) Magnitude error; (c) Phase angle; and (d) Phase angle error.

For this type of LED, the magnitude deviation between the developed TDM and the measured data is greater than Type A and B. However, considering the deviations in the magnitude, the median values are still generally small for components with larger magnitude, with larger deviations observed for harmonics with lower absolute values. The median values are lower than 10% for all harmonic orders. The deviations in the magnitude can be attributed to the simplification of the CCR functionality in the developed TDM, and the largest errors occur for the condition in which the harmonic current magnitude is smallest. In the model, the ability of the CCR to limit the current was idealized as a constant value, without considering finite response of control and error in regulation related to flow of current. The impact of this is evident in Figure A6 in Appendix A.3. On the other hand, reproduction of the harmonic phase angles by the Type C LED lamp TDM is very accurate and is insensitive to the harmonic order, unlike the Type A and B LED lamp TDMs (c.f. Figures 4d and 5d).

### 3.3.4. Type D

Details of the circuit model and its parameterization are included in Appendix A.4 and is presented for the first time in this paper. This includes full details of the power and control circuits and their parameters. Appendix A.4 also includes the model validation at the development test point, i.e., at rated ideal sinusoidal voltage.

A comparison of the range of harmonic current magnitude and phase angles across all considered test points is shown in Figure 7. As can be expected, the largest errors of the four LED lamp types are observed for this model. This can be attributed to the value of the LF current emissions, which, relative to fundamental component, are much smaller in comparison to all other LED lamp types (between 0–10% compared to approximately 0–90% for LED Type A, 0–40% for LED Type B, and 0–15% for LED Type C). Furthermore, the line current waveform of Type D LED lamps is sensitive to small errors in modeling the physical switched-mode driver, including, for instance, parasitic couplings, power components nonlinearity, and real signal transfer via control loop, which are difficult to derive and were not incorporated in the presented model. As the LF current emission magnitudes are small, these are extremely sensitive to variations in the power and control circuit, as well as the supply conditions. Although the relative deviations may be bigger, the absolute deviation is very small, due to the low magnitude values, and not as significant as for the other LED lamp types.

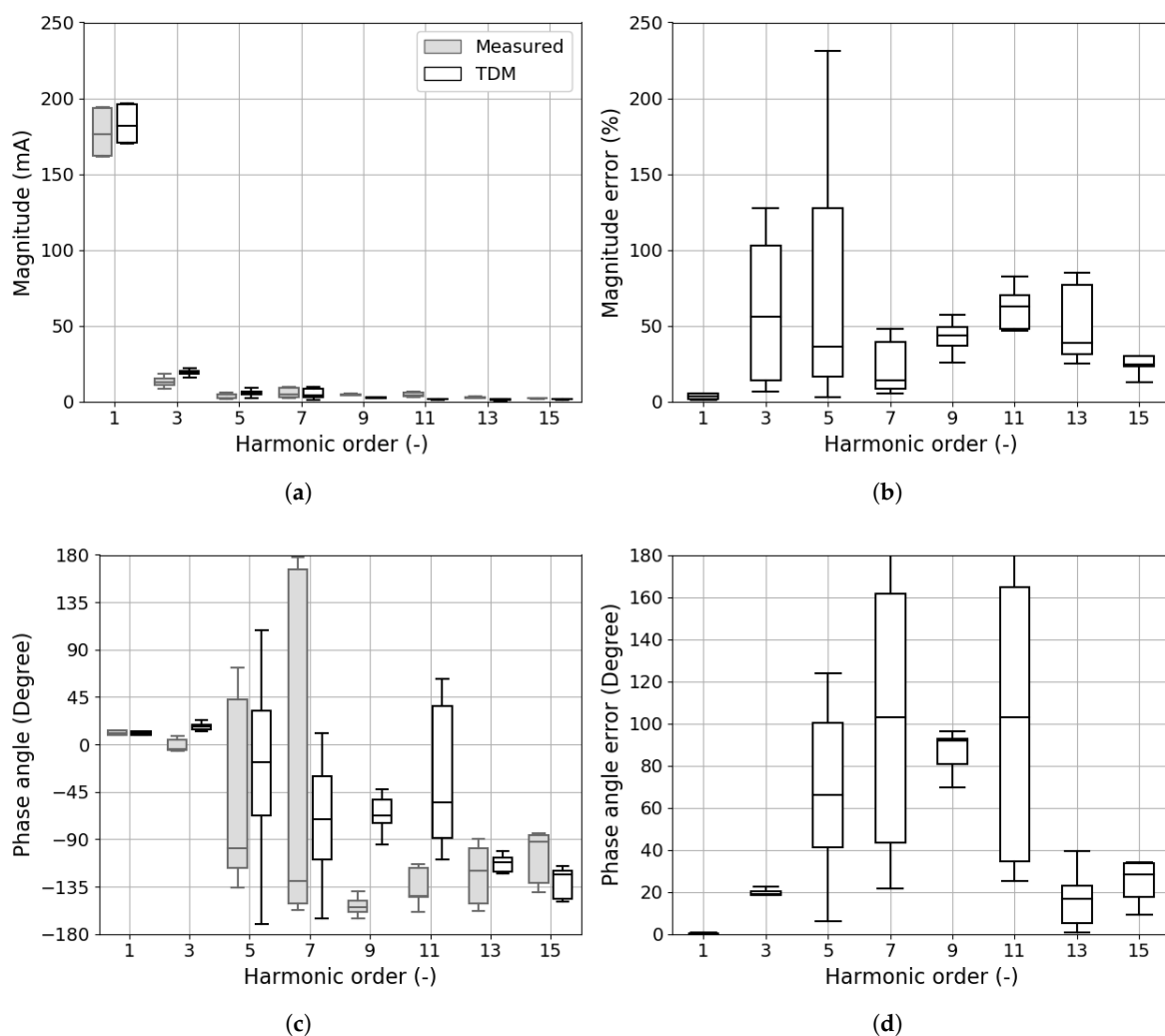


**Figure 7.** LED Type D: Comparison of the time-domain model (TDM) and the measured data for all test points: (a) Magnitude; (b) Magnitude error; (c) Phase angle; and (d) Phase angle error.

### 3.4. Total Distortion Indices

The total distortion indices, THD and THC, obtained from measurement and simulations and their deviations from the measured reference data, are presented in Figure 8. Again, this includes numeric values obtained for all test points.

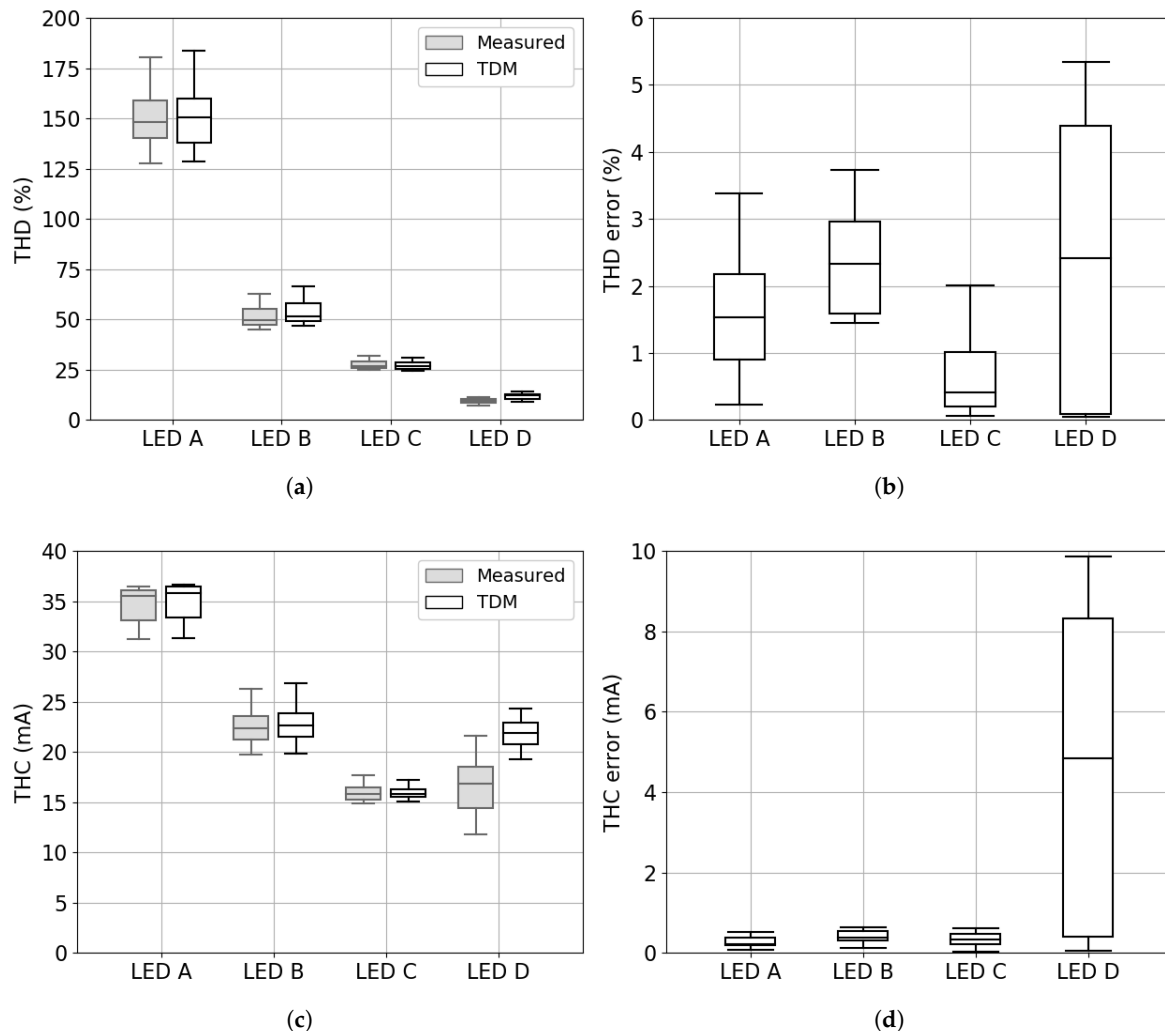


**Figure 8.** Comparison of the time-domain model (TDM) and the measured data for all test points: (a) THD; (b) THD error (absolute values); (c) THC; and (d) THC error (absolute values).

These results confirm the overall accuracy of the proposed TDMs and also serve to highlight the difference in the characteristics of the four general categories of LED lamps. For Type A LED lamps, the high values of THD and THC are both accurately reproduced by the TDM estimate, as it was previously shown that this model returns the lowest overall errors. Similar performance is observed for the Type B LED lamp. Even LED Type C and D lamps return reasonable errors for THD and THC in terms of absolute values. This indicates that the large errors observed are not coincident and occur in different supply voltage conditions, i.e., reducing the impact of individual larger errors on the overall assessment. The larger errors of the THC of the Type D LED lamp can be attributed to the small magnitude of the LF emissions which are generally overestimated by the TDM, but good accuracy of the THD is ensured by the dominant effect of the fundamental component, which is well represented by the model.

#### 4. Frequency Domain Modeling

Any power system component can be represented by a voltage controlled current source [3,11]:

$$I = f(V), \quad (5)$$

where  $I$  and  $V$  are vectors of harmonic phasors of the emitted current and the applied voltage, and the function  $f$  is a complex vector function.

If  $f$  is a non-linear function, a widely used and powerful technique is to linearize  $f$  around an operating base reference condition (e.g., the three voltage waveforms described in Section 2.2) [12].

Harmonic cross coupling and phase dependency can be elegantly modeled by estimating the direct and negative FCM  $Y^+$  and  $Y^-$ :

$$I = I_b + Y^+ \Delta V + Y^- \Delta V^*, \quad (6)$$

where  $I_b$  is the base current, i.e., the emission measured at the base reference conditions. The elements of the direct FCM  $Y^+$ , which accounts for direct and cross coupling between harmonic orders, and of the negative matrices FCM  $Y^-$ , which accounts for the background voltage "phase dependency", can be obtained either by numerical or laboratory tests, e.g., as described in [35].

The different FDMs used in this paper can be summarized starting from Equation (10).

##### *Constant Harmonic Current Source Model*

Constant harmonic current source models (CCM) are the simplest, and most commonly used, representation of a non-linear load. The load is modeled by a vector of constant current sources and are assumed independent of the background voltage distortion:

$$I = I_b. \quad (7)$$

##### *Decoupled Norton Models*

Decoupled Norton models (DNM) model only the interaction between applied harmonic voltages and emitted harmonic currents of the same order. In other words, the off-diagonal elements of  $Y^+$  are set to zero:

$$I = I_b + \text{diag}(Y^+) \Delta V. \quad (8)$$

##### *Coupled Norton Models*

Coupled Norton models (CNM) are able to take into account the cross coupling between different harmonic voltage and current orders but neglect the "phase dependency":

$$I = I_b + Y^+ \Delta V. \quad (9)$$

##### *Tensor Representation*

The tensor representation model (T2) is equivalent to the general model, as in Equation (10), but the direct and negative FCMs are represented by concise real-valued matrices in which elements are rank-2 tensors:

$$\Delta I = I - I_b = T2 \Delta V. \quad (10)$$

Representing  $\Delta I$  and  $\Delta V$  in Cartesian form, it is possible to write:

$$\begin{bmatrix} \begin{bmatrix} \Re(\Delta I_1) \\ \Im(\Delta I_1) \end{bmatrix} \\ \begin{bmatrix} \Re(\Delta I_2) \\ \Im(\Delta I_2) \end{bmatrix} \\ \vdots \\ \begin{bmatrix} \Re(\Delta I_H) \\ \Im(\Delta I_H) \end{bmatrix} \end{bmatrix} = \begin{bmatrix} \begin{bmatrix} \Re(I_1) \\ \Im(I_1) \end{bmatrix} \\ \begin{bmatrix} \Re(I_2) \\ \Im(I_2) \end{bmatrix} \\ \vdots \\ \begin{bmatrix} \Re(I_H) \\ \Im(I_H) \end{bmatrix} \end{bmatrix} - \begin{bmatrix} \begin{bmatrix} \Re(I_{b,1}) \\ \Im(I_{b,1}) \end{bmatrix} \\ \begin{bmatrix} \Re(I_{b,2}) \\ \Im(I_{b,2}) \end{bmatrix} \\ \vdots \\ \begin{bmatrix} \Re(I_{b,H}) \\ \Im(I_{b,H}) \end{bmatrix} \end{bmatrix} = \begin{bmatrix} T2_{1,1} & T2_{1,2} & \dots & T2_{1,K} \\ T2_{2,1} & T2_{2,2} & \dots & T2_{2,K} \\ \vdots & \vdots & \ddots & \vdots \\ T2_{H,1} & T2_{H,2} & \dots & T2_{H,K} \end{bmatrix} \times \begin{bmatrix} \begin{bmatrix} \Re(\Delta V_1) \\ \Im(\Delta V_1) \end{bmatrix} \\ \begin{bmatrix} \Re(\Delta V_2) \\ \Im(\Delta V_2) \end{bmatrix} \\ \vdots \\ \begin{bmatrix} \Re(\Delta V_K) \\ \Im(\Delta V_K) \end{bmatrix} \end{bmatrix}, \quad (11)$$

where  $H$  and  $K$  are highest considered current and voltage harmonic order, respectively.

The matrix elements of  $T2$ , i.e.,  $T2_{h,k}$ , can be determined using Fourier Descriptors [12,21,36,37]. The Fourier Descriptor is the discrete Fourier transform of a sequence of complex numbers,  $y(m_p)$ , represented by  $M_p$  evenly spaced vectors and is described by:

$$Y_{fd}[n] = \frac{1}{M_p} \sum_{m_p=1}^{M_p} y(m_p) e^{-jn \frac{2\pi(m_p-1)}{M_p}}, \quad (12)$$

where  $Y_{fd}[n]$  is the Fourier Descriptor of order  $n$ . Considering only the Fourier Descriptors of order 0 and -2  $Y_{fd}[0]$  and  $Y_{fd}[-2]$ , the matrix elements can be calculated as follows:

$$T2_{h,k} = \begin{bmatrix} y_{1,1} & y_{1,2} \\ y_{2,1} & y_{2,2} \end{bmatrix}_{h,k}, \quad (13)$$

$$y_{1,1} = \Re(Y_{fd}[0] + Y_{fd}[-2]), \quad (14)$$

$$y_{1,2} = -\Im(Y_{fd}[0] - Y_{fd}[-2]), \quad (15)$$

$$y_{2,1} = \Im(Y_{fd}[0] + Y_{fd}[-2]), \quad (16)$$

$$y_{2,2} = \Re(Y_{fd}[0] - Y_{fd}[-2]). \quad (17)$$

#### 4.1. Frequency Domain Model Development

The development of a FDM requires a huge number of tests in order to linearize the behavior of the lamps around a base operational point. In general, one test in the absence of perturbations is necessary to calculate the base currents spectra  $I_b$  (see Equation (10)). Then,  $N_1$  test values of the fundamental magnitude deviations from nominal are required to evaluate the first column of the direct matrix  $Y^+$ , and, for each background voltage harmonic considered (up to the  $K$ th odd harmonic order, where index  $k$  is used for voltage harmonics in order to distinguish from current harmonics index  $h$ ),  $N_2$  harmonic magnitudes, each characterized by  $N_3$  phase angles, have to be analyzed. The total number of tests is given by:

$$N_{tests} = 1 + N_1 + \frac{(K-1)}{2} \times N_2 \times N_3 \quad (18)$$

and is usually very large (from a few hundred to more than one thousand).

Depending on the kind of analysis to be performed, and on other practical issues, the tests can be performed either experimentally or numerically (i.e. starting from detailed TDMs). For example,

a detailed emission assessment of a specific device requires experimental testing, while a statistical distortion assessment of several kinds of devices can be performed using FDMs evaluated numerically starting from the more straightforward parameterization of TDM parameters, e.g., [25].

In this paper, the FDMs of the four LED lamps were obtained using the TDMs described and validated in the previous section. As the aim of this analysis was to compare the performance of the different FDMs for different LED driver circuits, the TDM are assumed to have acceptable accuracy, and their use allows for quicker development of FDMs than the measurement based approach.

To analyze the impact of the supply voltage waveform on the performance of the FDM, the FCMs were obtained by perturbing and linearizing the TDMs around the two operating points constituted by FT and PT voltage waveforms. For the sake of brevity, only harmonic orders up to the 15th were evaluated, and only the three dominant components ( $k = 3, 5, \text{and } 7$  for FT and  $k = 5, 7, \text{and } 11$  for PT) were considered in the modified distortion voltage waveforms. For the modified FT and PT voltage waveforms, simulations without perturbations were performed in order to evaluate the two base currents spectra  $I_b$ . For the harmonic perturbation, only one amplitude at a time was considered: for each of the dominant harmonic components, shown in Figure 3, the modified FT and PT, respectively, were amplified by a factor equal to 10%. The same 10% amplification factor was used for the components not present in the modified spectra (e.g., 3rd harmonic for PT), by first assuming their base amplitudes equal the limits suggested by standard EN 50160 [38], reported in Table 2. The number of phase angles, i.e.,  $M_p$  in Equation (12), selected was 24. Therefore, the total number of tests for each of the two different operating points was equal to 169 ( $N_1 = 0$ ,  $N_2 = 1$ ,  $K = 15$ , and  $N_3 = 24$  in Equation (18)).

**Table 2.** Harmonic voltage limits based on standard EN 50160.

k	3	5	7	9	11	13	15
Limit (%)	5	6	5	1.5	3.5	3	0.5

#### 4.2. Frequency Domain Model Assessment

FDM assessment was conducted by means of MC simulations. For each of the two operation points constituted by the modified FT and PT voltage waveforms, 100 MC trials were run. The perturbation added to the base spectrum was generated assuming a uniform distribution between 0 and 10% for harmonic magnitudes and a uniform distribution between 0 and  $2\pi$  for phase angles. As per the FDM derivation process, for the harmonic components not present in the modified FT and PT base cases, the random magnitude perturbation  $U \sim [0, 0.1 pu]$  was applied to the magnitudes of the limits reported in Table 2; for the MC simulations, the phase angle was randomly assigned from  $U \sim [0, 2\pi]$ .

#### 4.3. Results

From Sections 4.3.1–4.3.4, the results of the assessment are reported for each lamp category, comparing the performance of the four FDMs previously presented (CCM, DNM, CNM, and T2) with the TDM in terms of magnitude and phase angle and their errors. In addition to the magnitude and phase errors evaluated with Equations (1) and (2), the FDMs are also assessed analyzing the  $Y^+$  and  $Y^-$  matrices. In real terms,  $Y^+$  is able to take into account the linear direct and cross-coupling between voltage and current harmonic phasors, while  $Y^-$  takes into account the dependency of the current harmonics to the phase angle of the voltage harmonics. In the simple case of a linear system, the  $Y^+$  matrix is diagonal (no cross-coupling), while the  $Y^-$  matrix is nil. The following considerations apply:

- the T2 model is always more accurate, as it takes into account both  $Y^+$  and  $Y^-$ ;
- the CCM is as accurate as the other FDMs if the values of the  $Y^+$  and  $Y^-$  matrices are negligible;
- the DNM performance is comparable with the CNM and the T2 model if the off-diagonal elements of  $Y^+$  and of  $Y^-$  matrices are negligible; and
- the CNM performance is comparable with the T2 model if the  $Y^-$  matrix values tend to zero.

Finally, the comparison of the total distortion indicators, THD and THC, is shown in Section 4.3.5.

### 4.3.1. Type A

The performance of the different FDMs of the Type A LED lamp is shown for flat-top and peak-top supply voltage conditions in Figures 9 and 10, respectively.

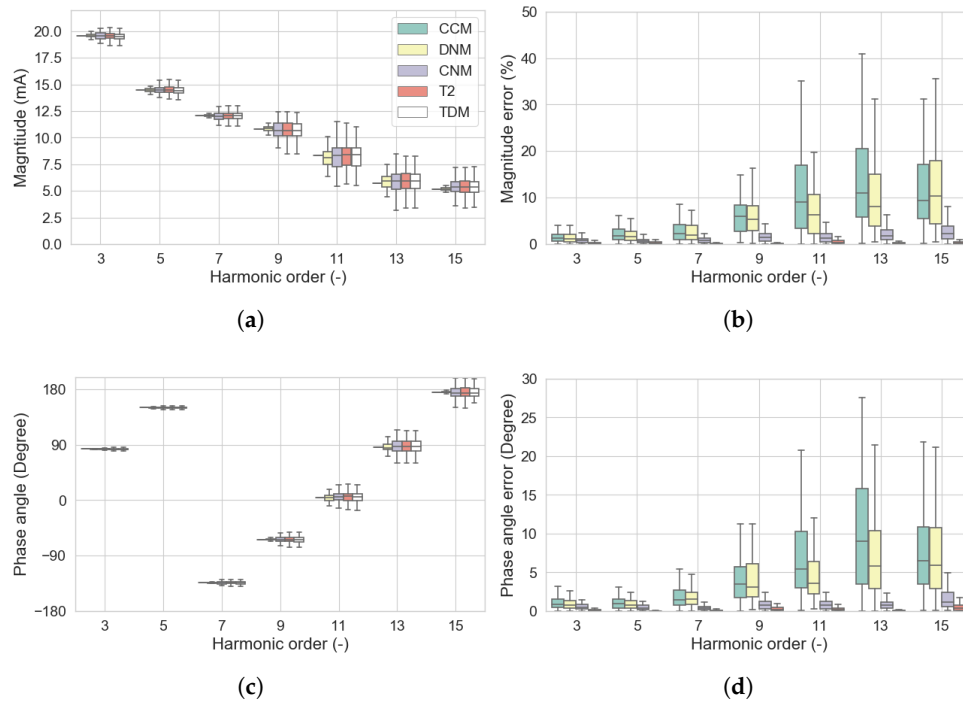


**Figure 9.** Comparison of the Type A LED lamp frequency domain models for flat-top voltage supply: (a) Magnitude; (b) Magnitude error; (c) Phase angle; and (d) Phase angle error.

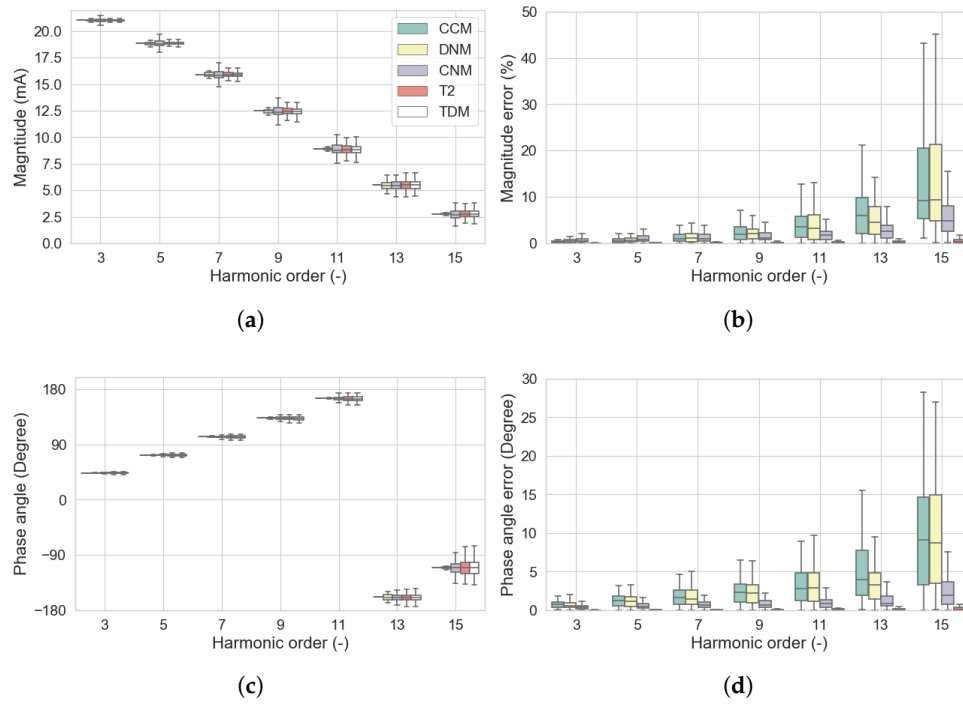


**Figure 10.** Comparison of the Type A LED lamp frequency domain models for peak-top voltage supply: (a) Magnitude; (b) Magnitude error; (c) Phase angle; and (d) Phase angle error.

In Figure 9a,b for flat-top (Figure 10a,b for peak-top), magnitudes and phase angles obtained by the four FDMs are compared to the results obtained by TDM using boxplots, with the exception of CCM, which is invariant with respect to the background harmonic voltage variations. In Figure 9c,d for flat-top (Figure 10c,d for peak-top), the corresponding relative and absolute errors are shown. The magnitude of the admittance matrices are shown in Figure 11 and are useful to help understand the performance of the different models.

It is possible to observe:

- the CNM and the T2 model perform noticeably better than the CCM and the DNM for both flat-top and peak-top voltage waveforms. This can be explained by the presence of non-negligible off-diagonal elements in both  $Y^+$  matrices (see Figure 11a,b);
- the T2 model performs significantly better than the CNM due to the non-negligible magnitudes of the elements of the  $Y^-$  matrices (see Figure 11c,d), although the magnitudes are about six times lower than the corresponding values of  $Y^+$  for both FT and PT;
- looking at Figure 11a,b, it is evident that in the case of PT supply condition the magnitudes of the elements of  $Y^+$  are smaller by a factor 3 compared to the FT supply condition; and
- the same considerations apply for phase angles. It should be noted that the phase angles returned by the FDMs are with respect to the cosine of the voltage waveform, rather than the sinusoid used in the TDM, so the angles presented here (and for the FDMs of other LED lamp types) cannot be directly compared with those in Section 3, but allow for a comparison between FDMs.

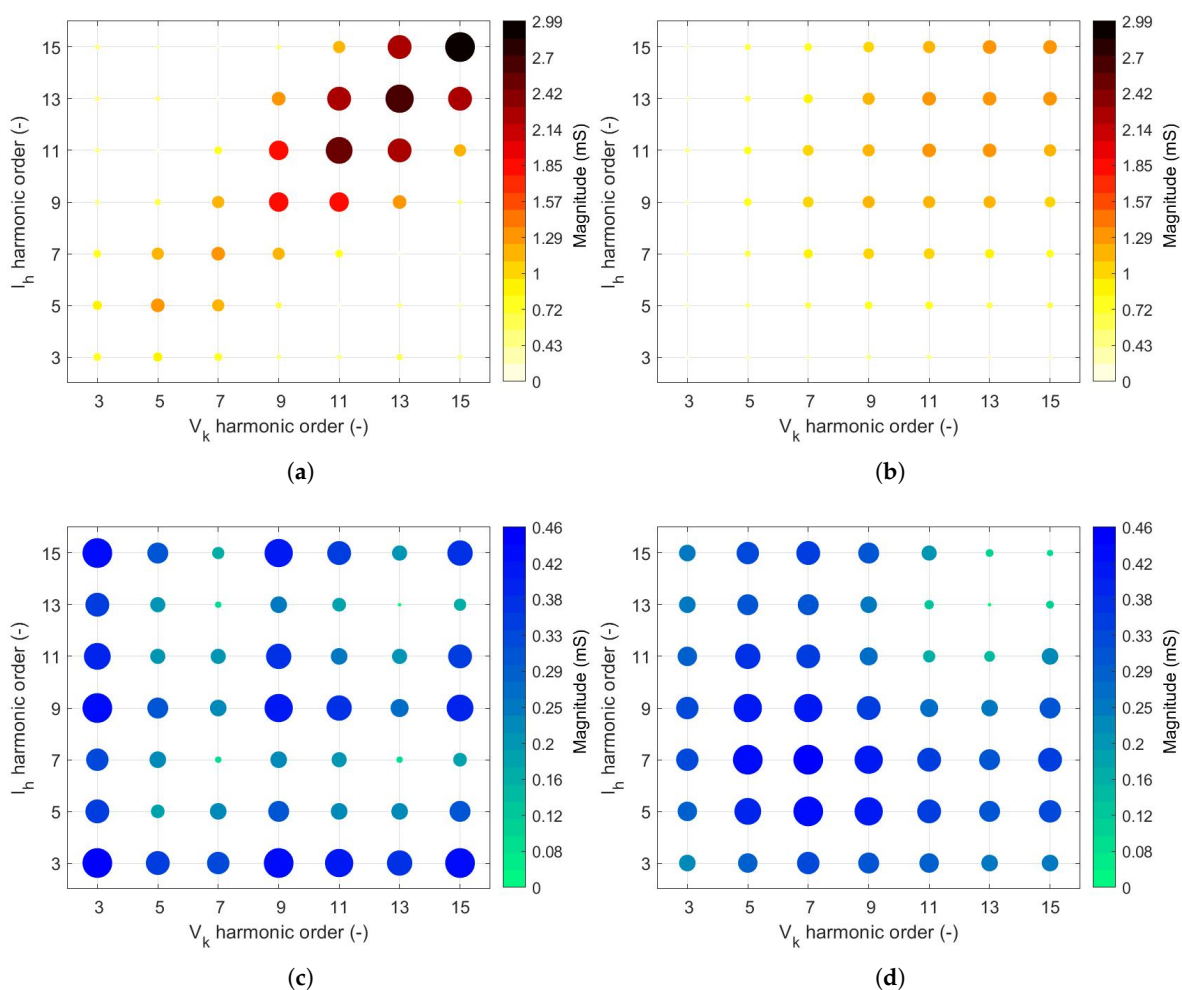


**Figure 11.** Magnitude of frequency coupling matrices of the Type A LED lamp: (a)  $Y^+$  FT; (b)  $Y^+$  PT; (c)  $Y^-$  FT; and (d)  $Y^-$  PT.

### 4.3.2. Type B

The performance of the different FDMs of the Type B LED lamp is shown for flat-top and peak-top supply conditions in Figures 12 and 13, respectively.

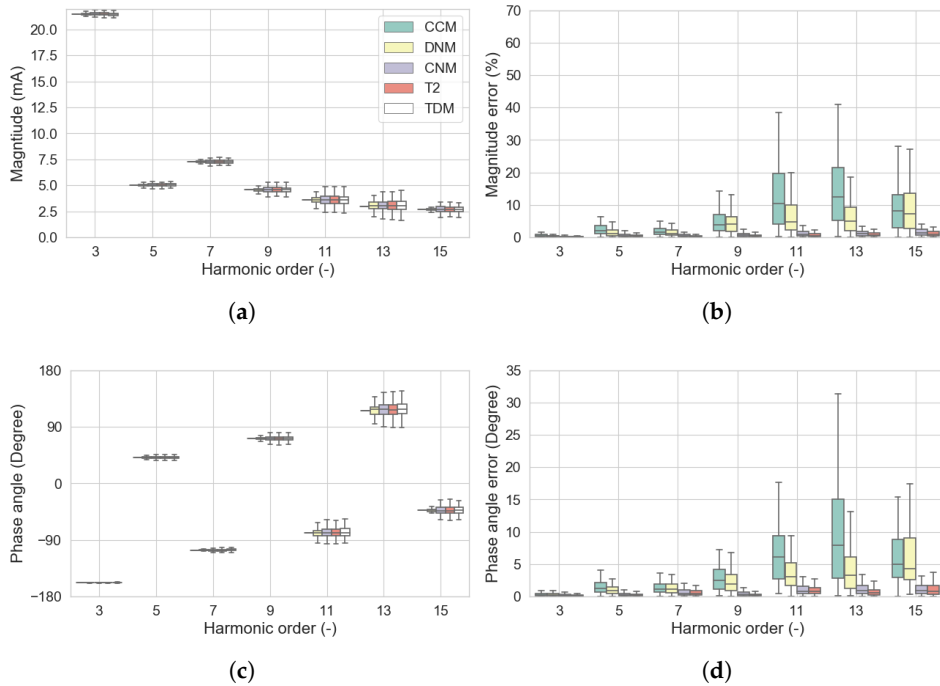


**Figure 12.** Comparison of the Type B LED lamp frequency domain models for flat-top voltage supply: (a) Magnitude; (b) Magnitude error; (c) Phase angle; and (d) Phase angle error.

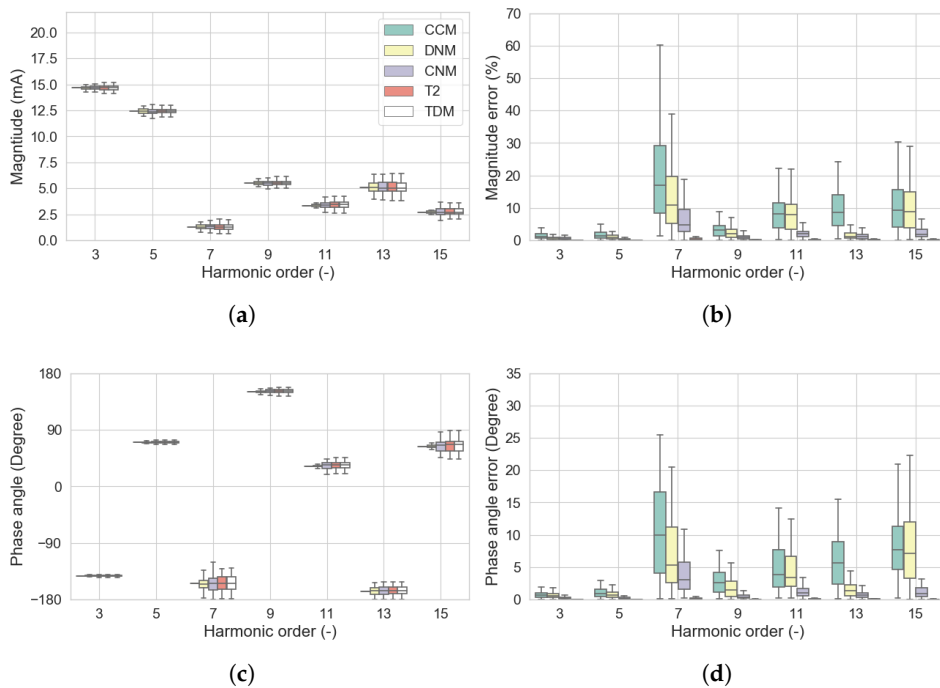


**Figure 13.** Comparison of the Type B LED lamp frequency domain models for peak-top voltage supply: (a) Magnitude; (b) Magnitude error; (c) Phase angle; and (d) Phase angle error.

Figures 12–14 are equivalent to those for the Type A LED lamp. It is possible to observe:

- $Y^+$  approaches a diagonal matrix, indicating that the most pronounced coupling exists between same order harmonics (e.g., between 11th and 11th) and between them and their nearest neighbors (e.g., between 11th and 9th and 13th), as can be seen in Figure 14a,b;
- moreover, the  $Y^+$  matrices are practically identical for both voltage waveforms (and also identical to that measured under ideal sinusoidal conditions [26]), which indicates that only one FCM is required to analyze both scenarios as already evidenced in [12];
- for this LED lamp, the CNM and the T2 model perform noticeably better than the CCM and the DNM for both FT and PT voltage waveforms, even if only a few off-diagonal elements of  $Y^+$  have non-zero values;
- although of similar magnitudes, the values of the  $Y^-$  for the PT voltage waveform are generally higher than those present in the  $Y^-$  for the FT voltage waveform, as demonstrated by the different level of accuracy between CNM and T2 in FT supply conditions in Figure 12c,d and in PT supply conditions in Figure 13c,d; and
- the same considerations apply for phase angles.

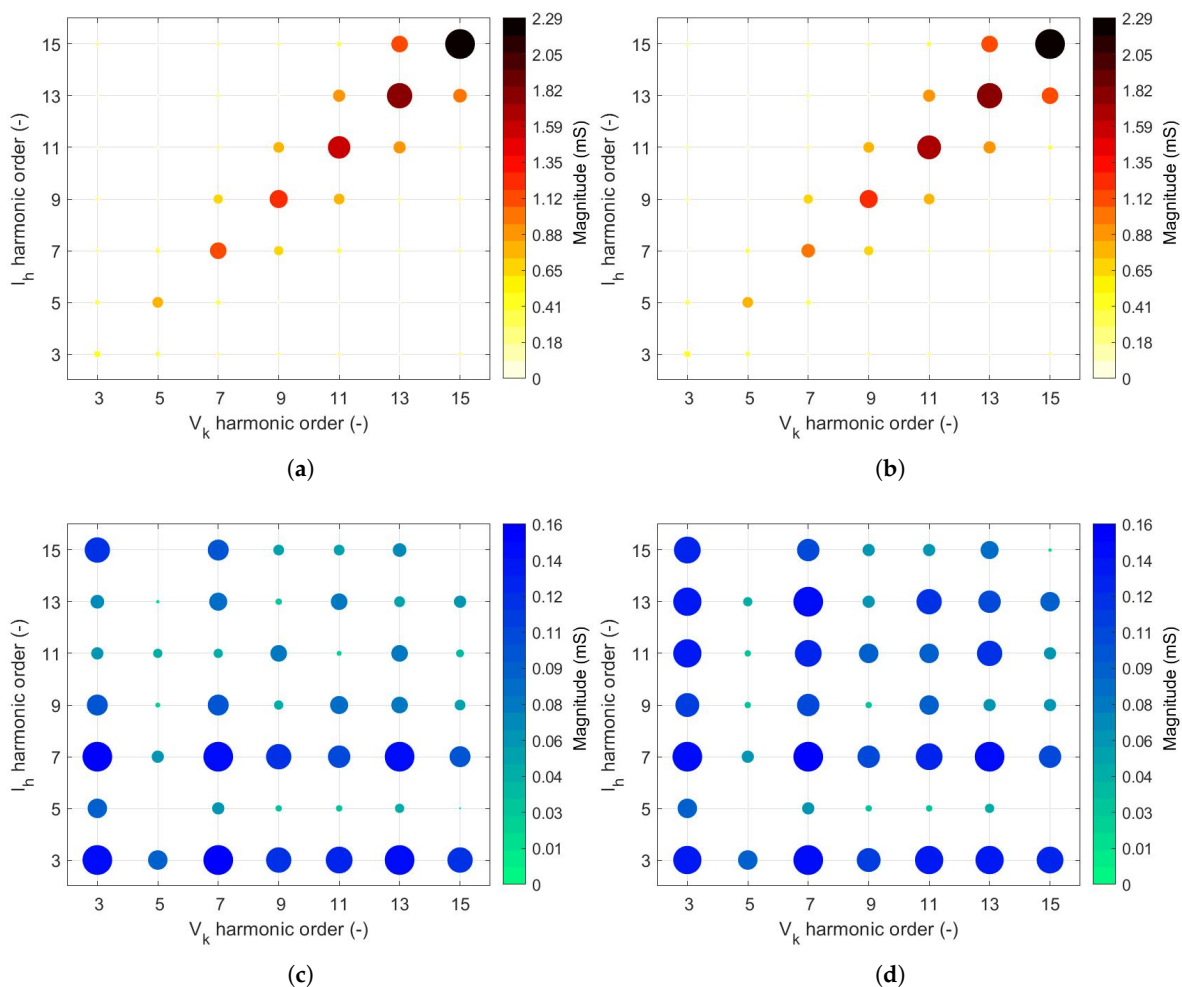


**Figure 14.** Magnitude of frequency coupling matrices of the Type B LED lamp: (a)  $Y^+$  FT; (b)  $Y^+$  PT; (c)  $Y^-$  FT; and (d)  $Y^-$  PT.

### 4.3.3. Type C

The performance of the different FDMs of the Type C LED is shown for flat-top and peak-top supply conditions in Figures 15 and 16, respectively.

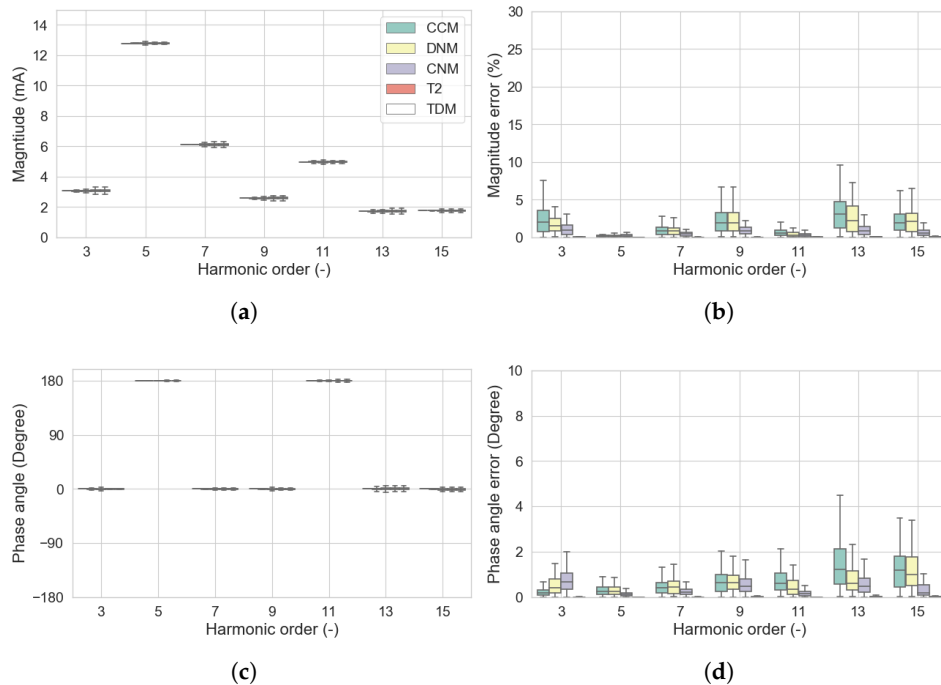


**Figure 15.** Comparison of the Type C LED lamp frequency domain models for flat-top voltage supply: (a) Magnitude; (b) Magnitude error; (c) Phase angle; and (d) Phase angle error.

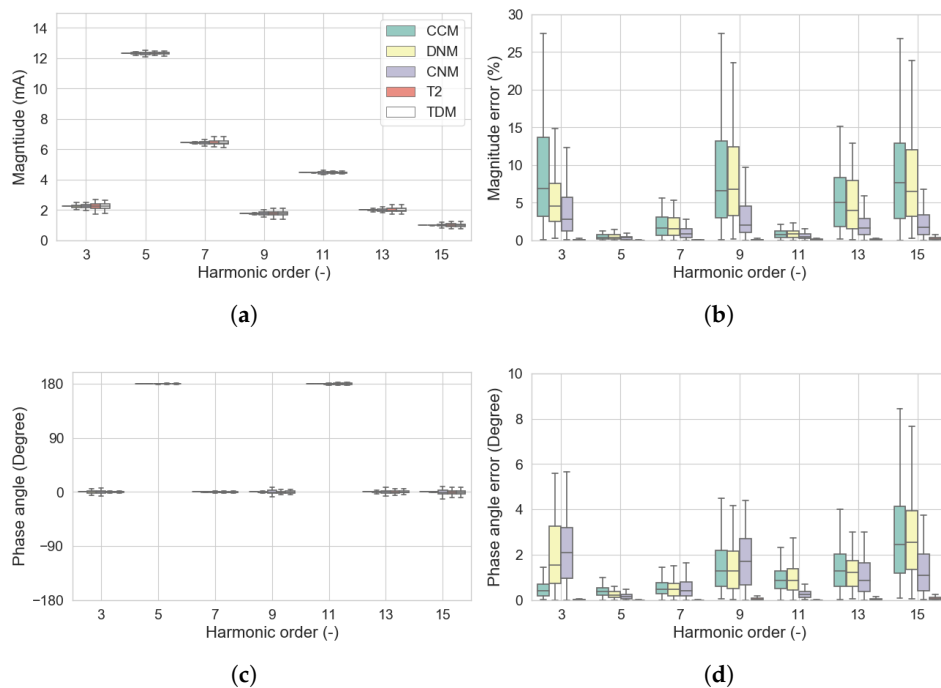


**Figure 16.** Comparison of the Type C LED lamp frequency domain models for peak-top voltage supply: (a) Magnitude; (b) Magnitude error; (c) Phase angle; and (d) Phase angle error.

Figures 15–17 are equivalent to those for Type A and B LED lamps.

It is possible to observe:

- the 'patterns' of both  $Y^+$  and  $Y^-$  are almost identical for both voltage waveforms, even if they have very small magnitudes compared with the other lamps;
- for the peak-top voltage waveform, all methods, except T2, show higher errors in respect to the FT supply condition due to the magnitudes of the elements being slightly greater (see Figures 15c,d and 16c,d);
- off-diagonal elements each two harmonic orders of  $Y^+$  are, in both cases, of the same order of magnitude of diagonal elements as evidenced by the great difference of performances between CCM and DNM versus CNM and T2; and
- the performance of the T2 model is significantly better than the other methods due to the order of magnitude of the elements of  $Y^-$ , which are the same as  $Y^+$ .

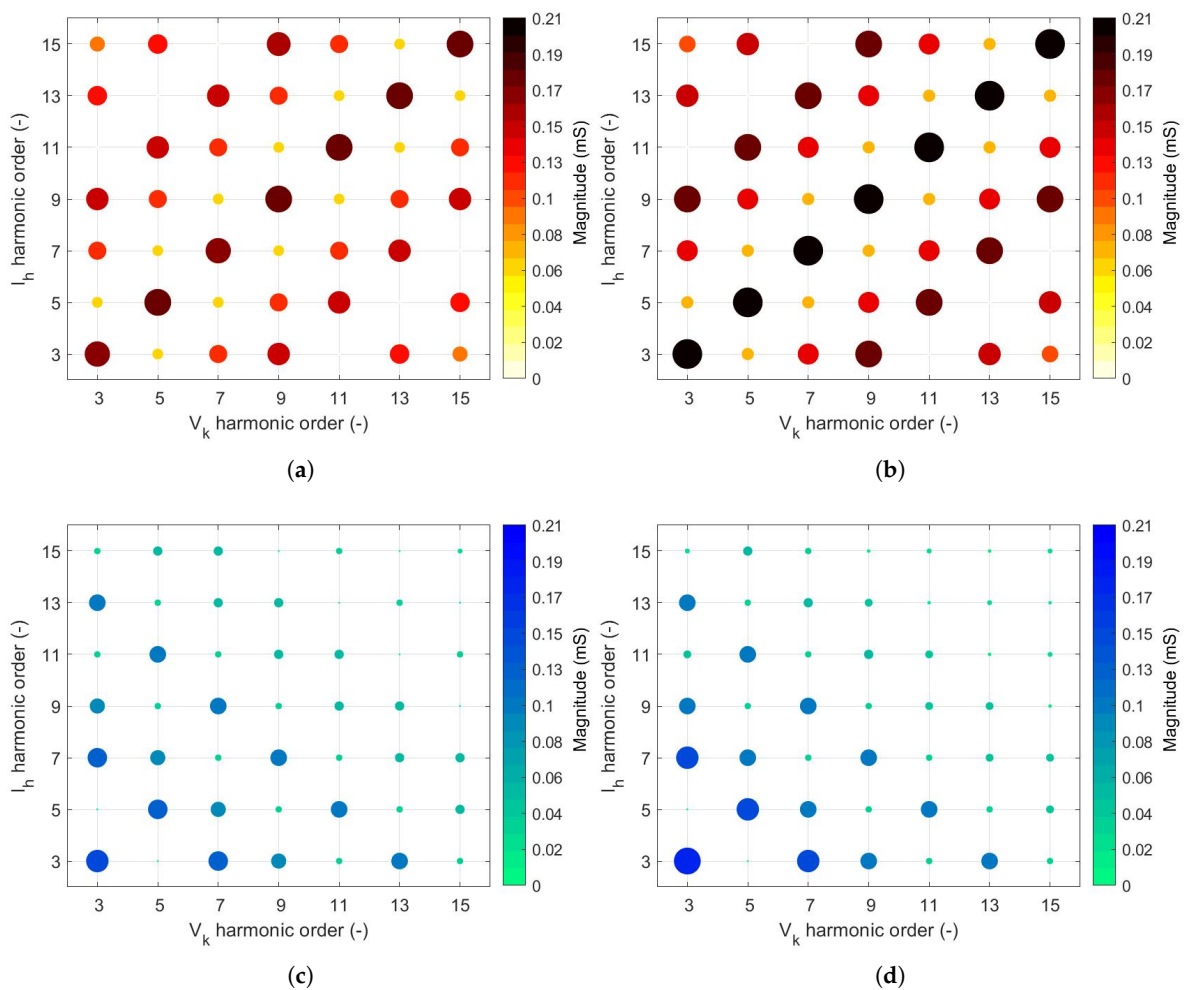


**Figure 17.** Magnitude of frequency coupling matrices of the Type C LED lamp: (a)  $Y^+$  FT; (b)  $Y^+$  PT; (c)  $Y^-$  FT; and (d)  $Y^-$  PT.

### 4.3.4. Type D

The performance of the different FDMs of the Type D LED lamp is shown for flat-top and peak-top supply conditions in Figures 18 and 19, respectively.

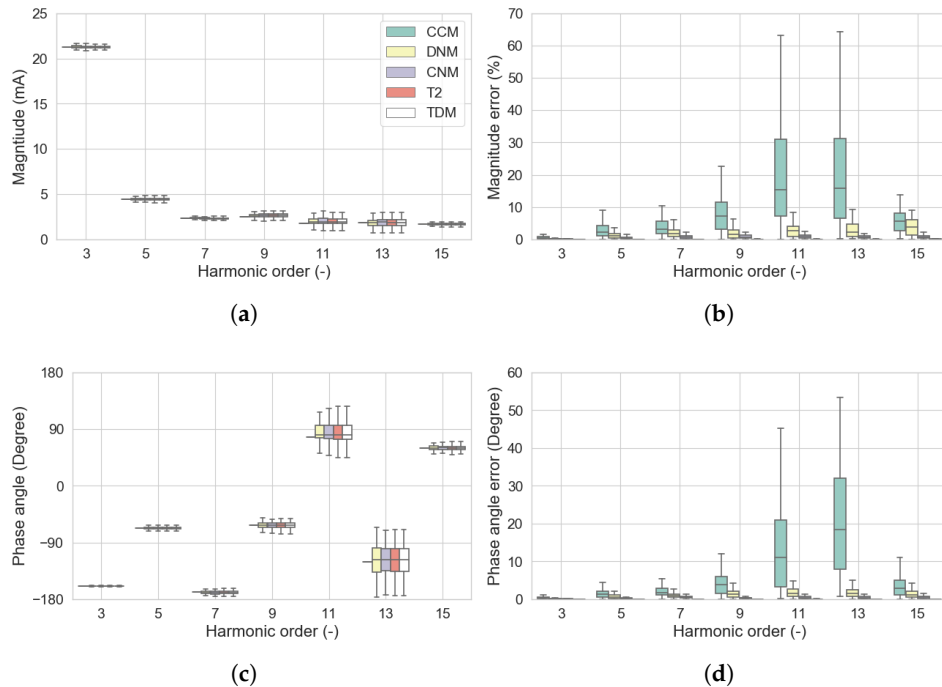


**Figure 18.** Comparison of the Type D LED lamp frequency domain models for flat-top voltage supply: (a) Magnitude; (b) Magnitude error; (c) Phase angle; and (d) Phase angle error.

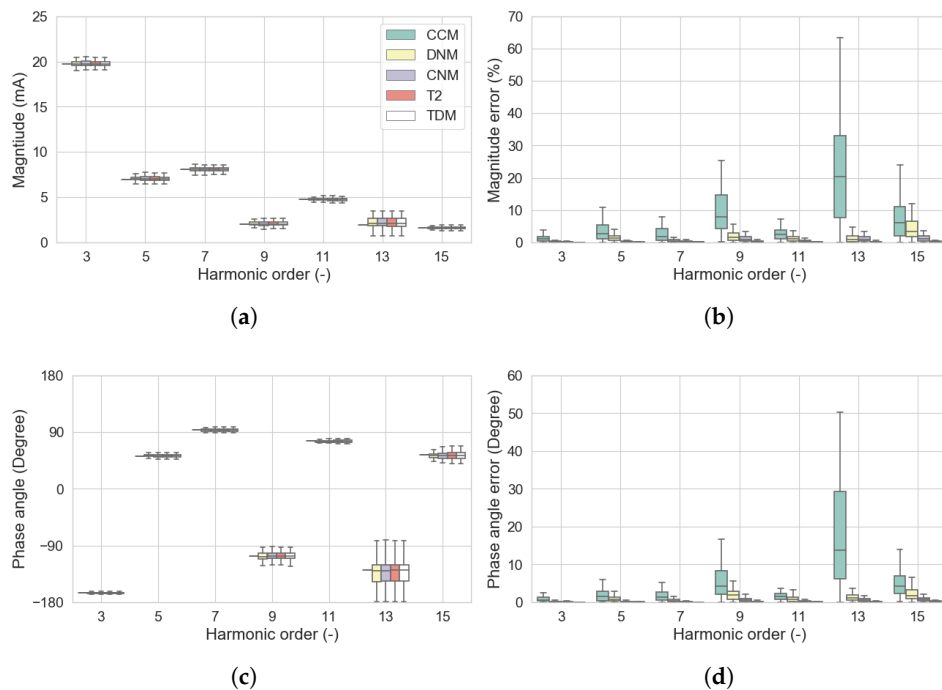


**Figure 19.** Comparison of the Type D LED lamp frequency domain models for peak-top voltage supply: (a) Magnitude; (b) Magnitude error; (c) Phase angle; and (d) Phase angle error.

Figures 18–20 are equivalent to those for Type A, B, and C LED lamps.

It is possible to observe:

- All FDMS, with the exception of the CCM, exhibit similar accuracy. This can be explained by analyzing  $Y^+$  in Figure 20 which is a diagonal matrix, indicating that the LED lamp behaves as a linear load and only direct coupling between same order harmonics exists;
- $Y^+$  are practically identical for both voltage waveforms;
- the aforementioned linear behavior can be modeled, for each harmonic, by a simple Norton equivalent constituted by a parallel RC circuit in parallel with a constant current source;
- $Y^-$  demonstrates that the sensitivity to the phase angle of the lower order harmonics is more pronounced, however, the values are generally two orders of magnitude lower than  $Y^+$ ; and
- for the PT voltage waveform, the magnitudes of the  $Y^-$  matrix are negligible for the 11th order harmonic current, which is reflected in the results in Figures 18 and 19, respectively, where the errors of the 11th harmonic are noticeably lower for the PT voltage waveform than the FT voltage waveform.

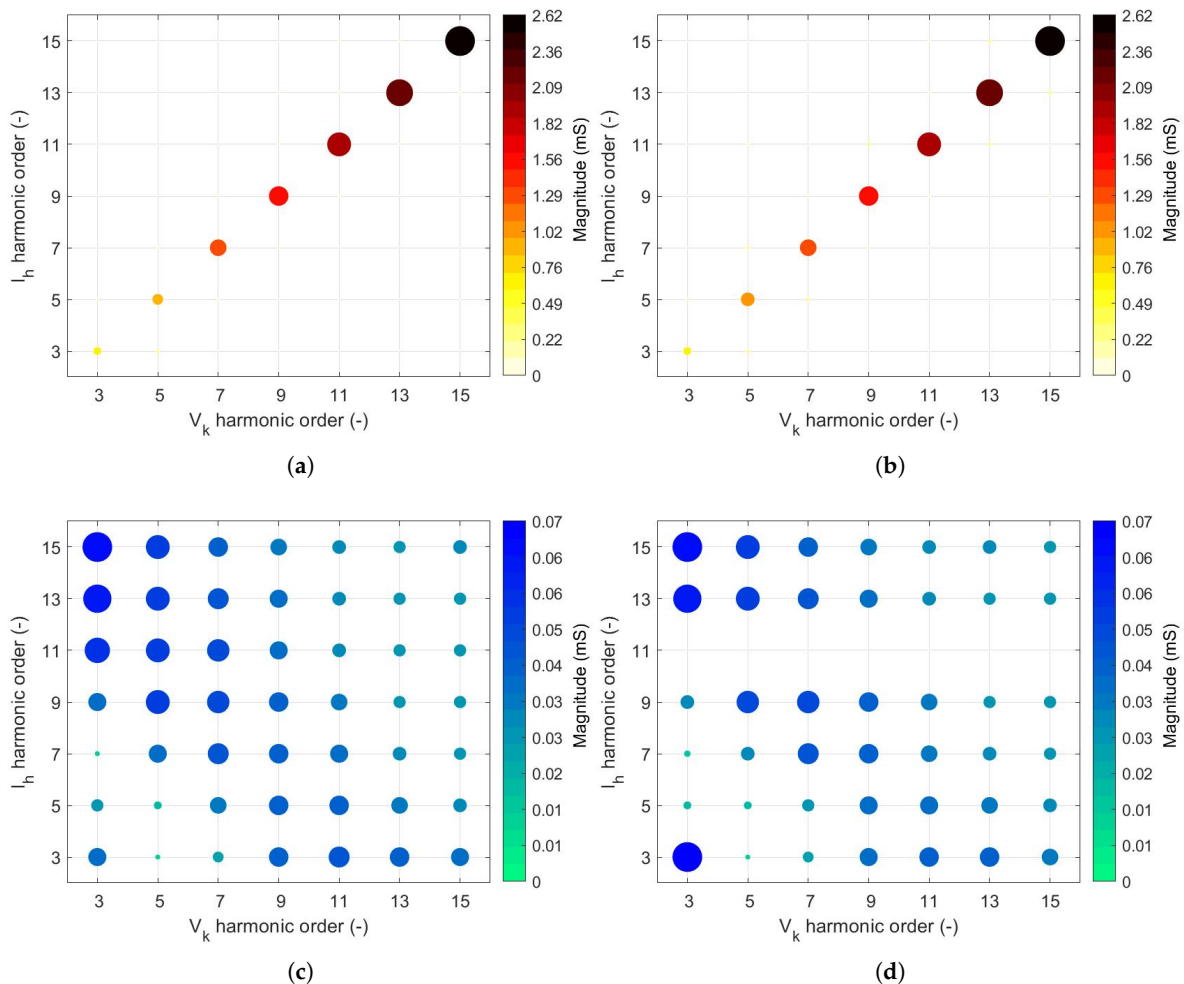


**Figure 20.** Magnitude of frequency coupling matrices of the Type D LED lamp: (a)  $Y^+$  FT; (b)  $Y^+$  PT; (c)  $Y^-$  FT; and (d)  $Y^-$  PT.

### 4.3.5. Total Distortion Indices

The total distortion indices THD and THC are reported in Figures 21 and 22.

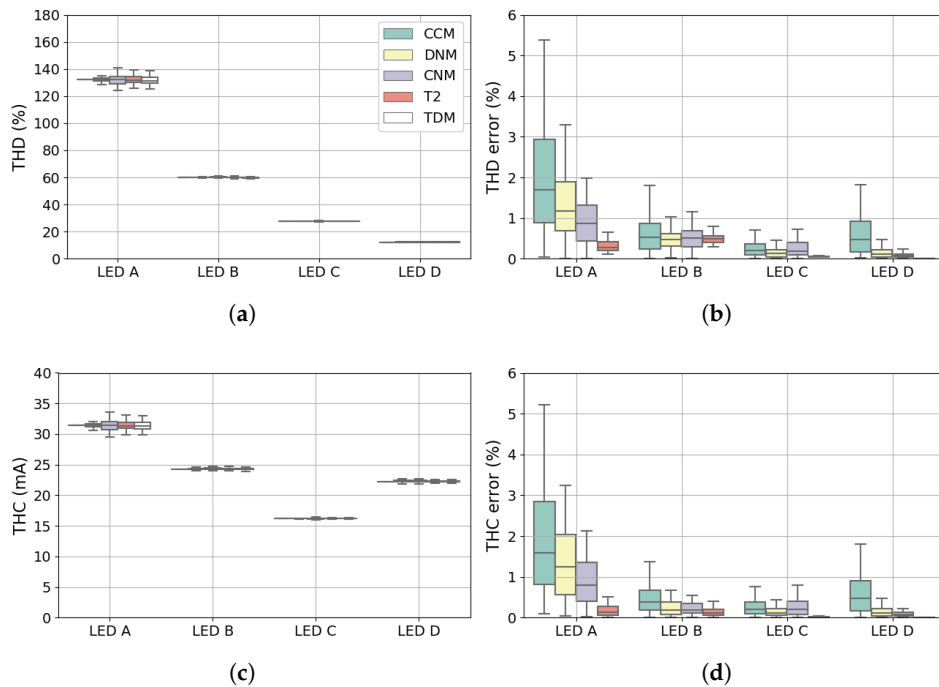


**Figure 21.** Comparison of the summary indices obtained with different frequency domain models supplied with flat-top voltage: (a) THD; (b) THD error (relative); (c) THC; and (d) THC error (relative).

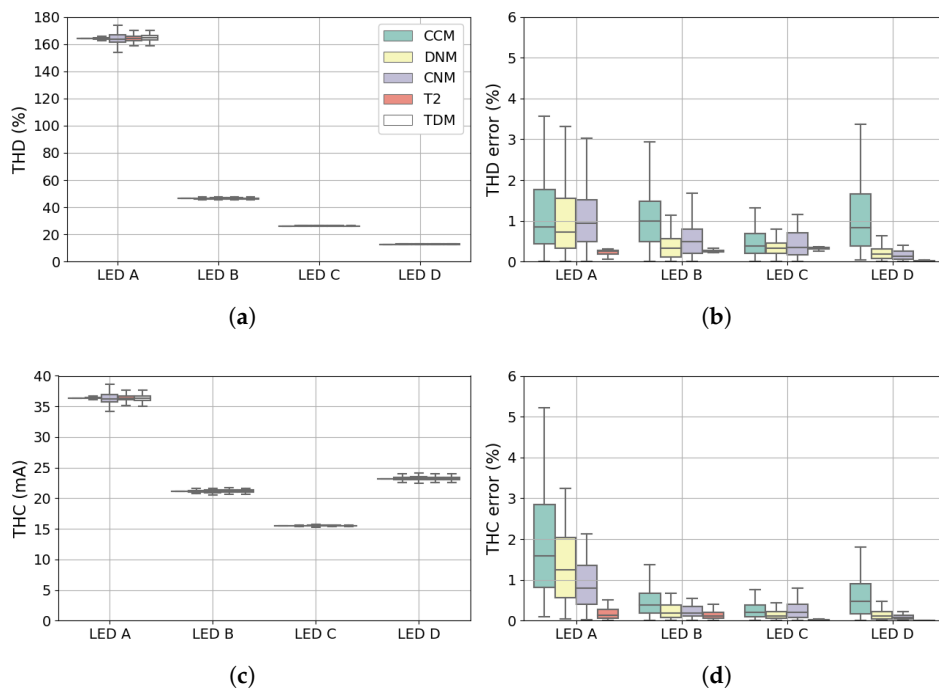


**Figure 22.** Comparison of the summary indices obtained with different frequency domain models supplied with peak-top voltage: (a) THD; (b) THD error (relative); (c) THC; and (d) THC error (relative).

The presented results confirm the overall improvement in the model performance with regard to the increase in model complexity. The performance of the simple CCM always results in the greatest

error, while the smallest reported errors are returned by the T2 model. Comparing the performance of the two Norton models, it is evident that they are sensitive to the type of LED lamp modeled and the presence of background voltage distortion; the decoupled model is generally able to perform as well as the coupled model (with respect to the total harmonic indices).

## 5. Conclusions

This paper provided a detailed analysis of two different modeling approaches for representing the LF current emissions of LED lamps: one in the time domain and one in the frequency domain. The considered approaches were illustrated using four general categories of LED lamps, which cover the vast majority of LED lamps currently available on the market. The aim was an in-depth assessment of the ability of commonly applied models to represent the LF current emissions of different categories of LED lamps. The performance of the models were quantitatively evaluated using experimental data, numerical simulations, and statistical analyses, thus providing comprehensive information about the overall accuracy that can be achieved in the general framework of harmonic penetration studies.

The main outcomes of the paper are:

- The TDMs, which in this paper were validated using experimental measurements, demonstrate that it is possible to achieve excellent levels of accuracy for certain types of LED lamps, i.e., Type A and B, in which control is either not present or can be emulated using an equivalent circuit form. For LED lamps that require specific representation of the control logic, i.e., Type C and Type D, new models were presented, for the first time, in this paper. For the Type C LED lamp example, the accuracy of the TDM is lower than Type A and Type B, but the median values are still very low with respect to measurements ( $< 10\%$ ). Higher magnitude errors are observed for the Type D LED lamp model but, in absolute terms, their values are very low. Areas of possible further improvement, e.g., by fine tuning the settings of the control algorithms, were discussed.
- The FDMs, which in this paper were derived from and compared against the TDMs, clearly show that the simulation error is significantly influenced by both the LED lamp type and the background voltage distortion. As expected, the overall errors reduce when increasing the model complexity; the magnitude errors obtained with the most complex model (i.e., the tensor based model T2) are always below 10%, and generally considerably lower (with median values of around a few percent or less), while the phase errors are always less than  $5^\circ$ , highlighting the value of including the phase dependency in the model formulation.
- The presented models and the quantitative results about their accuracy allow probabilistic harmonic penetration studies, such as the assessment of voltage distortion in LV networks and their future evolution, to be approached with the knowledge of the accuracy levels that can be obtained using different types of FDM.
- TDM parameter values were also reported in Appendix A for use by the community. From the presented TDMs, the FDMs analyzed in this paper can be obtained. Alternatively, the authors are happy to provide the parameters of the FDMs upon request.

**Author Contributions:** The author contributions are as follows: conceptualization, A.J.C., R.L., and A.T.; measurement, A.J.C. and S.Z.D.; modeling—frequency domain, A.J.C., R.L., A.T. and N.R.W.; modeling—time domain, A.J.C., S.Z.D., Z.G. and J.D.; writing—original draft preparation, A.J.C., S.Z.D., J.D., R.L. and A.T.; writing—review and editing, A.J.C., S.Z.D., J.D., R.L. and A.T. All authors have read and agreed to the published version of the manuscript.

**Funding:** The authors gratefully acknowledge financial support from the Italian Ministry of University and Research (PON03PE-00178-1) and the Technology Agency of the Czech Republic (project No. TN01000007).

**Acknowledgments:** The Authors wish to thank Xiao Xu for providing the measurement data.

**Conflicts of Interest:** The authors declare no conflict of interest. The funders had no role in the design of the study; in the collection, analyses, or interpretation of data; in the writing of the manuscript, or in the decision to publish the results.

## Appendix A. Time Domain Models and Parameters

Further details and component parameter values of the circuit models for LED Type A and B are available in [32,39].

### Appendix A.1. Type A LED Lamp

The typical Type A LED lamp driver circuit consists of an input resistor and electromagnetic interference (EMI) filter followed by a full-wave diode bridge rectifier (DBR) with smoothing bulk capacitor feeding a DC-DC converter to regulate the voltage across or the current through the LED chain. When considering the LF current emissions, this LED lamp can be represented by an equivalent circuit, shown in Figure A1, consisting of an input resistance  $R_{in}$ , input inductance  $L_{in}$ , a DBR, a DC link capacitor  $C_{dc}$ , and an equivalent load (in the form of a controlled current source), which represents the downstream DC-DC converter and LED chain. This simplification of the DC-DC converter and its output stage is possible due to the presence of the bulk  $C_{dc}$ , which decouples the rectifier stage from the rest of the circuit, in steady-state analysis and neglecting the high-frequency components of input current related to the DC-DC converter switching.

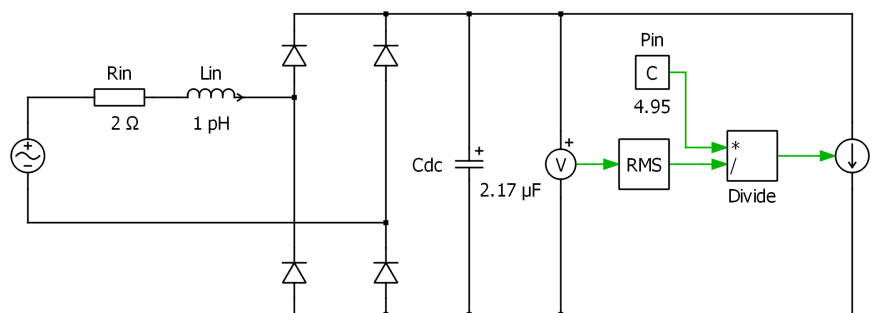


**Figure A1.** Time domain circuit model of the Type A LED lamp.

In the physical device, the DC-DC converter can be implemented with open- or closed-loop (OL/CL) feedback. If CL feedback is present, the equivalent load should take the form of a constant power load (used here and shown in Figure A1) or a constant current load. If OL feedback is present, then the equivalent load should be implemented as a constant resistance load. The presence of feedback can be identified using a sweep test of the fundamental voltage magnitude. The values of the circuit model parameters obtained by the parameter estimation technique, and valid for the analyzed Type A LED lamp introduced in Section 2.1, are marked directly on Figure A1. The performance of the model by means of its response to the rated ideal sinusoidal supply condition is documented in Figure A2.

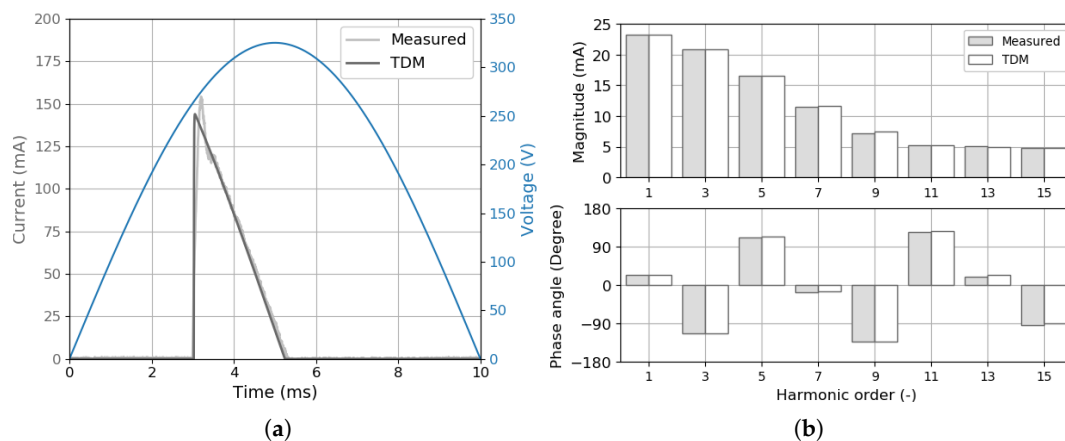


**Figure A2.** Comparison of measured data and the Type A LED lamp time-domain model (TDM) output at rated ideal sinusoidal condition: (a) Time domain. (b) Spectral components.

### Appendix A.2. Type B LED Lamp

The typical Type B LED driver circuit model consists of only a few passive components, with the full circuit model shown in Figure A3.

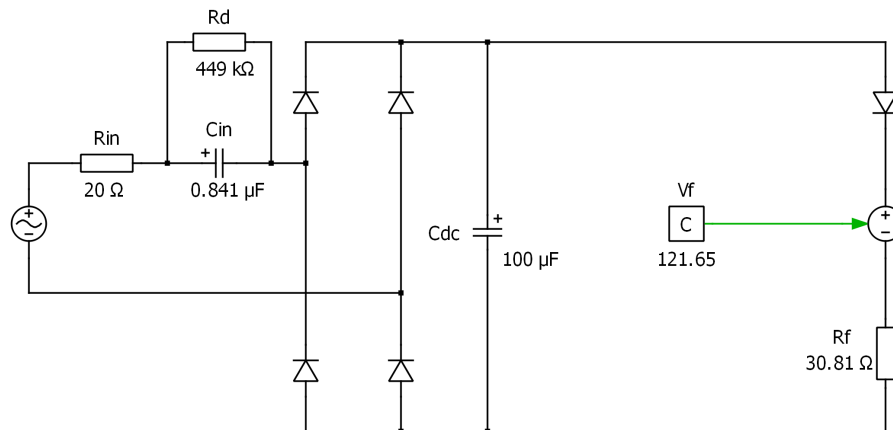


**Figure A3.** Time domain circuit model of the Type B LED lamp.

The feature of this circuit is the combination of two capacitors,  $C_{in}$  and  $C_{dc}$ , which form a capacitive divider across a DBR to reduce the supply voltage magnitude. Unlike the Type A LED lamp, the voltage ripple in the DC bus propagates to the LED string, and the LED string must be explicitly modeled with respect to the current-voltage characteristic of physical device. The LED string is modeled as an ideal diode, with constant DC voltage source, representing the forward voltage  $V_f$  of the LED string, and intrinsic resistance  $R_f$  connected in series. Due to the simple nature of the circuit, all component parameters are explicitly represented in the model and their values are marked directly on Figure A3. However, the discharging resistor  $R_d$  has no influence on the LF current emissions and is included only for the sake of completeness.

The performance of the model by means of its response to the rated ideal sinusoidal supply condition is documented in Figure A4.

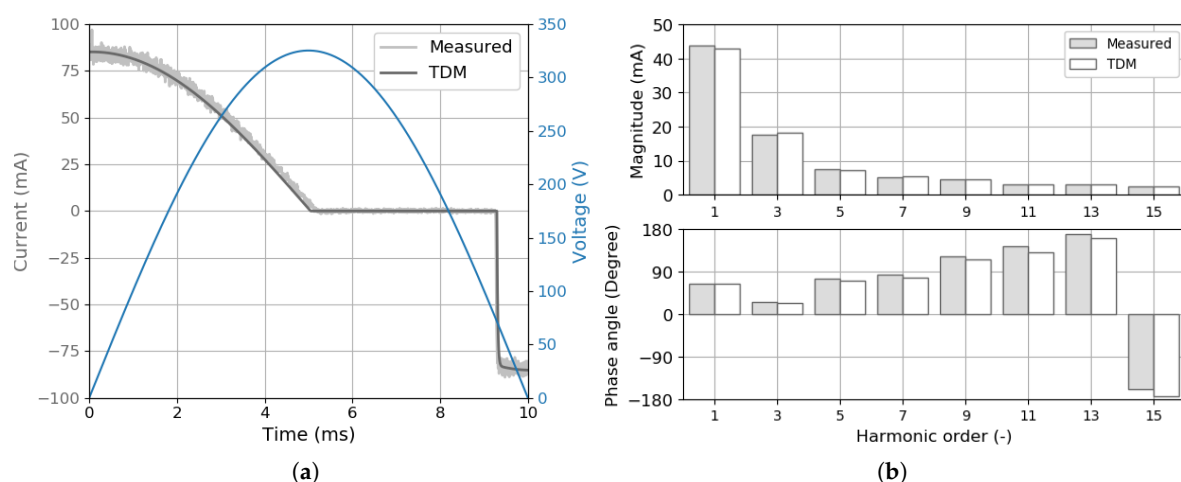


**Figure A4.** Comparison of measured data and the Type B LED lamp time-domain model (TDM) output at rated ideal sinusoidal condition: (a) Time domain. (b) Spectral components.

Appendix A.3. Type C LED Lamp

The Type C LED lamp driver circuit uses a DBR followed by a simple active DC-DC converter, in the form of a constant current regulator (CCR), to limit the output current through the series LED chain. The CCR is normally realized as an integrated circuit and is able to provide a constant current to the LED string over a wide voltage range.

In this circuit model, presented in Figure A5, the CCR behind the DBR is emulated using a controlled current source (CCS). The control logic and values are in Figure A5b. Due to boundary changes in the LED string operating point when the current changes from zero to the limit set by the CCR, and since DC current propagates directly to AC side, the LED string has to be modeled with respect to a real V-I curve of the LED string. In this case, the LED string is modeled as a part of CCS control by means of a calculated resistance, using the exponential-based approximation. In this model, forward voltage  $V_F$ , thermal potential including nonlinearity factor  $V_T$ , and  $R_F$  on-state resistance, representing the overall LED chain parameters, are considered. Starting from the calculated voltage over the LED string, when the LED current is reached, its value is limited to  $I_C$ , emulating the idealized action of the CCR. The model performance is given in Figure A6.

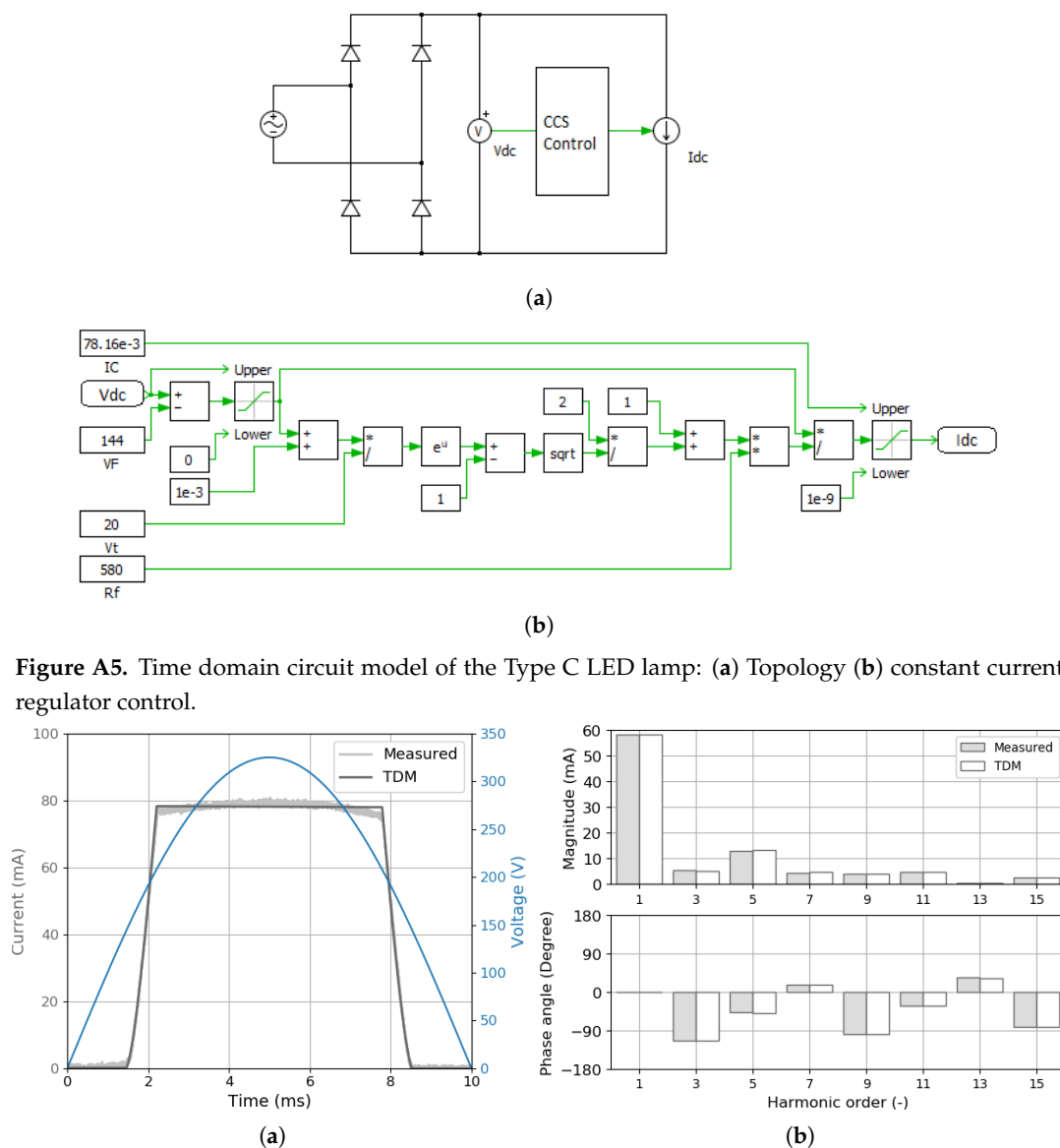


Figure A5. Time domain circuit model of the Type C LED lamp: (a) Topology (b) constant current regulator control.

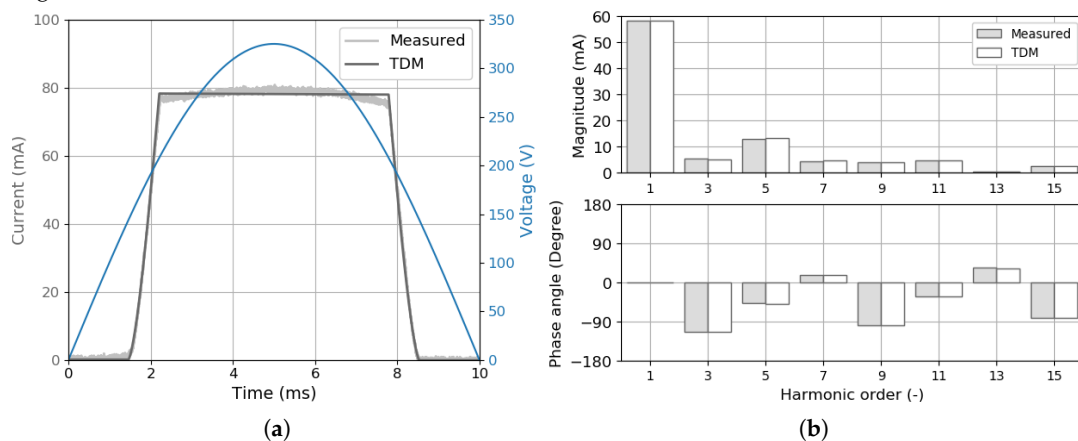


Figure A6. Comparison of measured data and the Type C LED lamp time-domain model (TDM) output at rated ideal sinusoidal condition: (a) Time domain. (b) Spectral components.

Appendix A.4. Type D LED Lamp

The Type D LED lamp driver circuit topology is similar to the Type A LED lamp driver, employing a passive full-bridge rectifier and at least one DC-DC converter stage. However, the input DC bus capacitor size is reduced, close to zero value, and the energy storage is moved to the output side of the DC-DC converter. This means that the DC-DC converter effect on the input line current waveform will be much higher and, in order to preserve its response, including the functionality of the control algorithm, a more detailed model of the DC-DC converter is required.

The Type D LED lamp driver circuit, including control logic and parametrization, were derived from the physical device by means of reverse engineering. This circuit consists of an offline single-stage flyback converter. The implemented and emulated PWM control is a peak current controller based on fixed switching frequency  $f_s$  with current slope compensation and constant output regulation without secondary feedback (utilizing an auxiliary winding to sense the output voltage). The  $f_s$  deduced from measurement is 60 kHz. The driver is designed for 0.7 A (20–56 V) output and for universal supply from 100–265 V at 50/60 Hz.

A circuit model of the driver, including the component parameter values, for simulation purposes is documented in Figure A7. The driver model consists of an input EMI filter model ( $C_4, L_1$ ), followed by an idealized DBR with small DC bus capacitor ( $C_2$ ) and consequent model of the flyback switching converter with CL output stage network ( $C_5, L_2+L_3$ ). The LED string is modeled by means of equivalent resistance ( $R_2$ ), possible due to the relatively small ripple in the output. Values of the control circuit parameters and the transformer are given in Tables A1–A3. The performance of the model by means of its response to the rated ideal sinusoidal supply condition is documented in Figure A8.

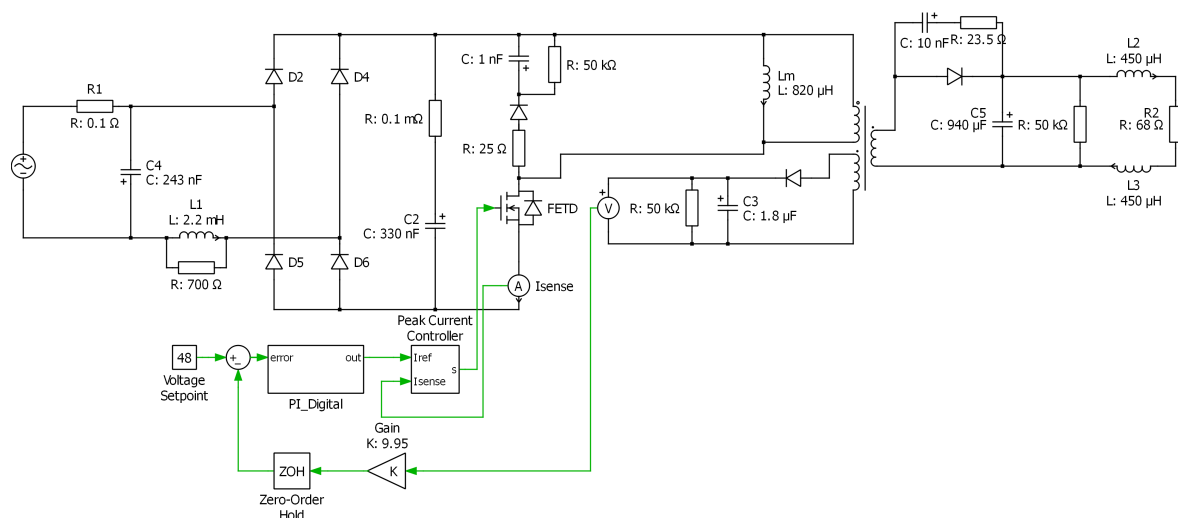


Figure A7. Time domain circuit model of the Type D LED lamp.

Table A1. LED Type D: Proportional Integral (PI) control parameters.

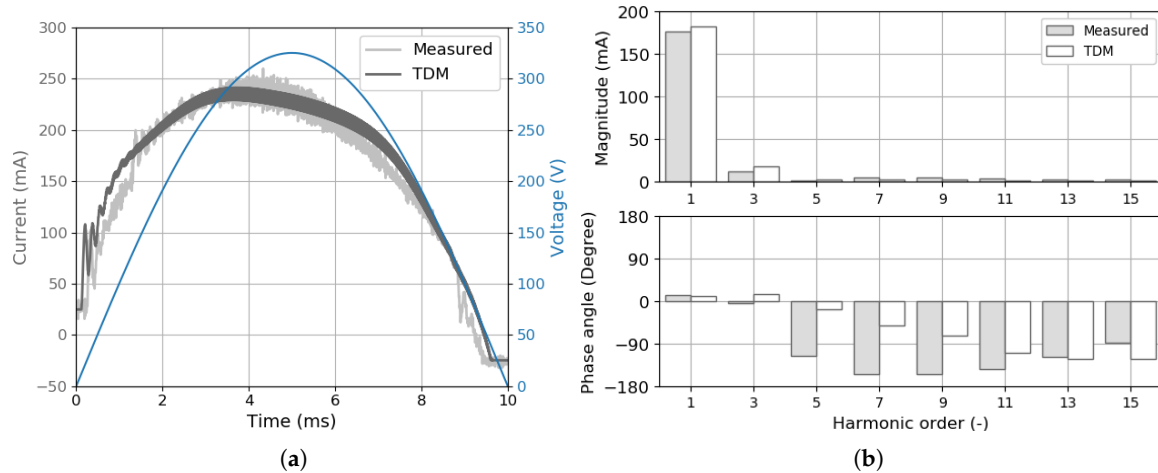
Kp	Ki	Ts	Usat	n	trd
0.0001	1/0.1	1e-6	10	7	0.002

Table A2. LED Type D: Peak current control parameters.

fs (kHz)	Min Duty Cycle (%)	Max Duty Cycle (%)	Slope Compensation (A)	Time Delay (s)
60	1	33	10	0

**Table A3.** LED Type D: Transformer parameters.

Windings	Turns	Polarity	Magnetization Inductance (H)	Initial Magnetization Current (A)
[2 1]	[ 120 -4 -36 ]	+	Inf	0

**Figure A8.** Comparison of measured data and the Type D LED lamp time-domain model (TDM) output at rated ideal sinusoidal condition: (a) Time domain. (b) Spectral components.

## References

- Gil-De-Castro, A.; Medina Gracia, R.; Ronnberg, S.K.; Blanco Castaneda, A.; Meyer, J. Differences in the performance between CFL and LED lamps under different voltage distortions. In Proceedings of the 18th IEEE International Conference on Harmonics and Quality of Power, Ljubljana, Slovenia, 13–16 May 2018.
- Collin, A.J.; Delle Femine, A.; Landi, C.; Langella, R.; Luiso M.; Testa, A. Assessment of the high frequency emissions of low-voltage electronic equipment under different supply conditions. In Proceedings of the 10th IEEE International Workshop on Applied Measurements for Power Systems, Aachen, Germany, 25–27 September 2019.
- Medina, A.; Segundo-Ramirez, J.; Ribeiro, P.; Xu, W.; Lian, K.L.; Chang, G.W.; Dinavahi, V.; Watson, N.R. Harmonic analysis in frequency and time domain. *IEEE Trans. Power Del.* **2013**, *28*, 1813–1821. [[CrossRef](#)]
- Yanchenko, S.; Meyer, J. Harmonic emission of household devices in presence of typical voltage distortions. In Proceedings of the IEEE PowerTech Conference, Eindhoven, Holland, 29 June–2 July 2015.
- Blanco, A.M.; Yanchenko, S.; Meyer, J. Impact of supply voltage distortion on the harmonic emission of electronic household equipment. In Proceedings of the 2013 VII Simposio Internacional sobre la Calidad de la Energía Eléctrica—SICEL, Medellín, Colombia, 27–29 November 2013.
- Xu X.; Collin, A.J.; Djokic, S.Z.; Yanchenko, S.; Moller, F.; Meyer, J.; Langella, R.; Testa, A. Analysis and modeling of power-dependent harmonic characteristics of modern PE devices in LV networks. *IEEE Trans. Power Del.* **2017**, *32*, 1014–1023.
- Cresswell, C. Steady State Load Models for Power System Analysis. Ph.D. Thesis, The University of Edinburgh, Edinburgh, UK, 2009.
- Rylander, M.; Grady, W.M.; Arapostathis, A.; Powers, E.J. Power Electronic Transient Load Model for Use in Stability Studies of Electric Power Grids. *IEEE Trans. Power Syst.* **2010**, *25*, 914–921. [[CrossRef](#)]
- Du, Y.; Lu, D.D.-C.; James, G.; Cornforth, D.J. Modeling and analysis of current harmonic distortion from grid connected PV inverters under different operating conditions. *Sol. Energy* **2013**, *94*, 182–194. [[CrossRef](#)]
- Kukacka, L.; Dupuis, P.; Simanjuntak, R.; Zissis, G. Simplified models of LED ballasts for spice. In Proceedings of the 2014 IEEE Industry Application Society Annual Meeting, Vancouver, BC, Canada, 5–9 October 2014; pp. 1–5.
- Arrillaga, J.; Smith, B.C.; Watson, N.R.; Wood, A.R. *Power System Harmonic Analysis*; Wiley: New York, NY, USA, 1997.

12. Caicedo, J.E.; Romero, A.A.; Zini, H.C.; Langella, R.; Meyer, J.; Watson, N.R. Impact of Reference Conditions on the Frequency Coupling Matrix of a Plug-in Electric Vehicle Charger. In Proceedings of the 18th IEEE International Conference on Harmonics and Quality of Power, Ljubljana, Slovenia, 13–16 May 2018.
13. Ramirez, A.; Rico, J.J. Harmonic/State Model-Order Reduction of Nonlinear Networks. *IEEE Trans. Power Del.* **2016**, *31*, 1379–1387.
14. Kwon, J.B.; Wang, X.; Blaabjerg, F.; Bak, C.L.; Wood, A.R.; Watson, N.R. Harmonic Instability Analysis of a Single-Phase Grid-Connected Converter Using a Harmonic State-Space Modeling Method. *IEEE Trans. Ind. Appl.* **2016**, *52*, 4188–4200. [[CrossRef](#)]
15. Kwon, J.B.; Wang, X.; Blaabjerg, F.; Bak, C.L.; Sularea, V.S.; Busca, C. Harmonic Interaction Analysis in a Grid-Connected Converter Using Harmonic State-Space (HSS) Modelling. *IEEE Trans. Power Electron.* **2017**, *32*, 6823–6835. [[CrossRef](#)]
16. Larsen, E.; Baker, D.; McIver, J. Low-order harmonic interactions on ac/dc systems. *IEEE Trans. Power Del.* **1989**, *4*, 493–5019. [[CrossRef](#)]
17. Fauri, M. Harmonic modeling of non-linear load by means of crossed frequency admittance matrix. *IEEE Trans. Power Syst.* **1997**, *12*, 1632–16387. [[CrossRef](#)]
18. Sun, Y.; Zhang, G.; Xu, W.; Mayordomo, J.G. A harmonically coupled admittance matrix model for AC/DC converters. *IEEE Trans. Power Syst.* **2007**, *22*, 1574–1582. [[CrossRef](#)]
19. Lehn, P.W.; Lian, K.L. Frequency coupling matrix of a voltage source converter derived from piecewise linear differential equations. *IEEE Trans. Power Del.* **2007**, *22*, 1603–1612. [[CrossRef](#)]
20. Smith, B.C.; Watson, N.R.; Wood, A.R.; Arrillaga, J. Harmonic tensor linearisation of HVDC converters. *IEEE Trans. Power Del.* **1998**, *13*, 1244–1250. [[CrossRef](#)]
21. Watson, N.R.; Scott, T.L.; Hirsch, S.J.J. Implications for distribution networks of high penetration of compact fluorescent lamps. *IEEE Trans. Power Del.* **2009**, *24*, 1521–1528. [[CrossRef](#)]
22. Yong, J.; Chen, L.; Nassif, A.B.; Xu, W. A frequency-domain harmonic model for compact fluorescent lamps. *IEEE Trans. Power Del.* **2010**, *25*, 1182–1189. [[CrossRef](#)]
23. Molina, J.; Sainz, L. Model of electronic ballast compact fluorescent lamps. *IEEE Trans. Power Del.* **2014**, *29*, 1363–1371. [[CrossRef](#)]
24. Molina, J.; Mesas, J.J.; Mesbahi, N.; Sainz, L. LED lamp modeling for harmonic studies in distribution systems. *IET Gen. Trans. Distrib.* **2017**, *11*, 1063–1071. [[CrossRef](#)]
25. Guo, Z.; Djokic, S.Z.; Xu, X.; Collin, A.J.; Langella, R.; Testa, A. Parameterised component-based models for harmonic analysis of aggregate LED lamp loads. In Proceedings of the 19th IEEE International Conference on Harmonics and Quality of Power, Dubai, UAE, 22–25 March 2020. [[CrossRef](#)]
26. Collin, A.J.; Drapela, J.; Langella, R.; Testa, A.; Djokic, S.Z.; Watson, N.R. Harmonic modeling of LED lamps by means of admittance frequency coupling matrices. In Proceedings of the IEEE PowerTech Conference, Milan, Italy, 23–27 June 2019.
27. Blanco, A.M.; Parra, E.E. Effects of high penetration of CFLs and LEDs on the distribution networks. In Proceedings of the 14th IEEE International Conference on Harmonics and Quality of Power, Bergamo, Italy, 26–29 September 2010.
28. Xu, X.; Collin, A.; Djokic, S.Z.; Langella, R.; Testa, A.; Drapela, J. Experimental evaluation and classification of LED lamps for typical residential applications. In Proceedings of the IEEE PES Innovative Smart Grid Technologies Conference Europe (ISGT-Europe), Torino, Italy, 26–29 September 2017.
29. Collin, A.; Djokic, S.; Drapela, J.; Langella, R.; Testa, A. Light flicker and power factor labels for comparing LED lamp performance. *IEEE Trans. Ind. Appl.* **2019**, *55*, 7062–7070.
30. Arias, M.; Vazquez, A.; Sebastian, J. An overview of the AC-DC and DC-DC converters for LED lighting applications. *Automatika* **2012**, *53*, 156–172. [[CrossRef](#)]
31. *Electromagnetic Compatibility (EMC)—Part 4-13: Testing and Measurement Techniques—Harmonics and Interharmonics Including Mains Signalling at a.c. Power Port, Low Frequency Immunity Tests*; IEC 61000-4-13:2002 + AMD1:2009 + AMD2:2015; CEI-IEC: Geneva, Switzerland, 2015. [[CrossRef](#)]
32. Xu, X. Harmonic Modeling and Characterisation of Modern Power Electronic Devices in Low Voltage Networks. Ph.D. Thesis, The University of Edinburgh, Edinburgh, UK, 2018.
33. Xu, X.; Gunda, J.; Fang, D. Modelling and aggregation of LED lamps for network harmonic analysis. In Proceedings of the Power Systems Computation Conference (PSCC), Dublin, Ireland, 11–15 June 2018.

34. *Testing and Measurement Techniques – General Guide on Harmonics and Interharmonics Measurements and Instrumentation, for Power Supply Systems and Equipment Connected Thereto*; IEC 61000-4-7, 2002 + A1:2009; CEI-IEC: Geneva, Switzerland, 2009.
35. Gallo, D.; Langella, R.; Luiso, M.; Testa, A.; Watson, N.R. A new test procedure to measure power electronic devices' frequency coupling admittance. *IEEE Trans. Instrum. Meas.* **2018**, *67*, 2401–2409.
36. Langella, R.; Testa, A.; Caicedo, J.E.; Romero, A.A.; Zini, H.C.; Meyer, J.; Watson, N.R. On the use of fourier descriptors for the assessment of frequency coupling matrices of power electronic devices. In Proceedings of the 18th IEEE International Conference on Harmonics and Quality of Power, Ljubljana, Slovenia, 13–16 May 2018.
37. Frater, L. Light Flicker and Harmonic Modeling of Electrical Lighting. Ph.D. Thesis, University of Canterbury, Canterbury, New Zealand, 2015.
38. *Voltage Characteristics of Electricity Supplied by Public Distribution Networks*; CENELEC, Standard EN 50160; CENELEC: Brussels, Belgium, 2013.
39. Guo, Z. Harmonic Load Modeling of Residential Customers in Low-Voltage Networks. Master's Thesis, University of Edinburgh, Edinburgh, UK, 2019.

**Sample Availability:** All of the models are available upon request from the authors.



© 2020 by the authors. Licensee MDPI, Basel, Switzerland. This article is an open access article distributed under the terms and conditions of the Creative Commons Attribution (CC BY) license (<http://creativecommons.org/licenses/by/4.0/>).